



Article submitted to journal

Subject Areas:

quantum annealing and optimisation,
quantum phase transitions,
disordered systems, open quantum
systems

Keywords:

quantum tunnelling, Kibble-Zurek
Scaling, transverse Ising models,
quantum spin glass, Griffiths
singularities, p-spin models,
decoherence, antiferromagnetic
interactions, NP-complete and
NP-hard problems

Author for correspondence:

Atanu Rajak

e-mail: atanu.physics@presiuniv.ac.inQuantum Annealing: An
Overview

Atanu Rajak¹, Sei Suzuki², Amit Dutta³
and Bikas K. Chakrabarti^{4,5}

¹ Presidency University, Kolkata -700073, India² Saitama Medical University, Moroyama, Saitama
350-0495, Japan³ Indian Institute of Technology Kanpur, 208016, India⁴ Saha Institute of Nuclear Physics, 1/AF Bidhannagar,
Kolkata-700064, India⁵ Indian Statistical Institute, 203 B. T. Road,
Kolkata-700108, India

In this review, after providing the basic physical concept behind quantum annealing (or adiabatic quantum computation), we present an overview of some recent theoretical as well as experimental developments pointing to the issues which are still debated. With a brief discussion on the fundamental ideas of continuous and discontinuous quantum phase transitions, we discuss the Kibble-Zurek scaling of defect generation following a ramping of a quantum many body system across a quantum critical point. In the process, we discuss associated models, both pure and disordered, and shed light on implementations and some recent applications of the quantum annealing protocols. Furthermore, we discuss the effect of environmental coupling on quantum annealing. Some possible ways to speed up the annealing protocol in closed systems are elaborated upon: We especially focus on the recipes to avoid discontinuous quantum phase transitions occurring in some models where energy gaps vanish exponentially with the system size.

1. Introduction

Following the recent technological advance in manipulation of a quantum state, the notion of quantum computation and simulation which initially stemmed from pure theoretical concepts has now spread to flourish an industry with an immense possibility of technological applications. In particular, studies of quantum annealing (QA) have gained a tremendous momentum since programmable QA machines, dubbed as quantum annealers, with more than thousands of qubits have been realized and commercialized. In this review, having provided an overview of QA protocol, we discuss some recent theoretical and experimental developments of the QA exploiting the advantage of utilizing quantum tunneling in finding the minimum of a classical energy function.

QA is usually aimed at seeking the ground state of a generic Ising model, which may contain random biases and/or random many-body interactions [1–3]. Many optimization problems including the traveling salesman problem, job scheduling problem, knapsack problem, and so on, are shown to reduce to this problem. Therefore the application of QA extends from physics to our daily life. This broadness of application is another reason why QA is attracted much attention in industry. Now, let us consider an Ising model denoted by the Hamiltonian H_P , where the subscript P stands for the problem Hamiltonian. We assume that H_P is a classical many-body Ising Hamiltonian described in terms of the z components of the Pauli operator $\{\sigma_j^z\}$. We further introduce a driver Hamiltonian H_D which is not commutative with H_P and has the trivial ground state. A simple choice for H_D is the transverse field: $H_D = -\sum_j \sigma_j^x$, so that H_D does not commute with H_P . The total Hamiltonian of QA is given as

$$H(t) = A(t)H_D + B(t)H_P, \quad (1.1)$$

where $A(t)$ and $B(t)$ are the scheduling function satisfying $A(t_i) \gg B(t_i)$ at the initial time t_i and $A(t_f) \ll B(t_f)$ at the final time t_f so that $H(t)$ interpolates between H_D at $t = t_i$ and H_P at $t = t_f$. The initial state at $t = t_i$ is set at the ground state of $H_D \approx H(t_i)/A(t_i)$. If the change in $H(t)$ with t is “sufficiently” small, the spin state evolves adiabatically (i.e., stays in the ground state of the instantaneous Hamiltonian) and arrives at the ground state of H_P at $t = t_f$ which we seek. This constitutes the basic notion of the QA, also known as the adiabatic quantum computation [4–10]. Throughout this paper, we shall employ QA scheme using the transverse Ising Hamiltonian (if not otherwise mentioned). To illustrate, we consider the following Hamiltonian with ferromagnetic nearest neighbour interactions in one dimension:

$$H = -J \sum_j \sigma_j^z \sigma_{j+1}^z - \Gamma \sum_j \sigma_j^x. \quad (1.2)$$

where J denotes the strength of the interaction and Γ is the strength of the non-commuting transverse field. Here $H_D = -\sum_j \sigma_j^x$ and $H_P = -\sum_j \sigma_j^z \sigma_{j+1}^z$. The transverse field Γ is annealed to reach the ground state of H_P from the ground state of H_D .

The success of QA is determined by how slowly the Hamiltonian changes with time. According to the adiabatic theorem of quantum mechanics, the criterion of the adiabatic time evolution is given by [11]

$$\frac{\max \left[\left| \langle 1(t) | \frac{dH(t)}{dt} | g(t) \rangle \right| \right]}{\min[\Delta(t)]^2} \ll 1, \quad (1.3)$$

where $|g(t)\rangle$ and $|1(t)\rangle$ are the instantaneous ground and first-excited states at time t , respectively, and $\Delta(t)$ denotes the instantaneous energy gap above $|g(t)\rangle$. The min and max functions are taken with respect to the variable t . Thus, roughly speaking, QA works better for larger $\Delta(t)$ [12].

As a classical counterpart to QA, simulated annealing (SA) is a known method of computation for optimization problems [13]. In this method, we prepare the Gibbs-Boltzmann distribution of H_P at sufficiently high temperature by means of the Monte-Carlo method and literally anneal the system down to zero temperature. If annealing is sufficiently slow, then we are expected to arrive at the ground state of H_P with high probability. SA utilizes the thermal fluctuation

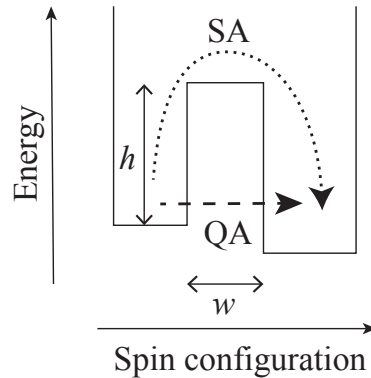


Figure 1. Schematic picture of the thermal fluctuation and quantum tunneling in a system with local energy minima separated by an energy barrier with the height h and the width w .

for optimization, which induces the thermal (Arrhenius) jump from a local energy minimum to another separated by an energy barrier. The escape rate from a local minimum over the energy barrier with height h is given by $e^{-h/k_B T}$, where k_B and T denote the Boltzmann constant and the temperature. Assuming that h is proportional to the system size N , this suggests that an exponentially long time in N is necessary to reach the global energy minimum by SA.

In contrast to SA, quantum tunneling induces an escape from a local minimum through an energy barrier as shown schematically in Fig. 1. The tunneling probability is approximately given by $e^{-\sqrt{\hbar}w/g}$ [14,15], where g denotes the strength of quantum fluctuation which corresponds to the transverse field Γ in transverse Ising models. Therefore, assuming the height $h \sim O(N)$ and the width $w < O(N^{1/2})$, the time necessary to escape from a local minimum due to quantum tunneling is subexponential in N . For such a system, quantum tunneling helps the system to equilibrate even though the system is glassy, i.e., non-ergodic in the absence of the quantum fluctuation, leading to a potential advantage of QA over SA in glassy systems. This role of quantum tunneling was first discussed by Ray et al., in 1989 [16] (see discussions in [17]) in this regard) in the context of the restoration of the replica symmetry or ergodicity due to quantum fluctuation in the quantum version of the Sherrington-Kirkpatrick model [18], which is detailed in the next section. Although the existence of an energy landscape with thin and high barriers in specific models is still an issue of debate, it must be a foundation for the speedup of QA over SA [17,19]. In addition, several numerical and experimental studies have provided evidences for such an advantage of QA over SA in some specific models as shown in Secs. 1(b)i and 2. We show a brief time-line for the development of QA in Fig. 2.

The review is organized in the following fashion: Having discussed the basic idea behind the QA scheme and the results for various models in the context of annealing and defect generation especially for annealing across a quantum critical point in Sec. 1, we move to discuss various implementations of annealing protocols in Sec. 2. In Sec. 3, we probe how does coupling to an external environment influence the QA process. In Sec. 4, we again refer to the close systems and discuss possible ways to speed QA processes especially in the context of avoiding discontinuous phase transitions. Some recent applications are discussed in Sec. 5.

(a) Quantum phase transition and quantum annealing

The minimum gap $\min[\Delta(t)]$ appearing in Eq. (1.3) often decreases with increasing the number of spins. In general the energy gap vanishes at a quantum phase transition (QPT) because a QPT separates disordered and ordered phases and the ground state is degenerate at a transition. Let us consider the transverse Ising Hamiltonian introduced in Eq. (1.2). The initial state, for $\Gamma \gg J$,

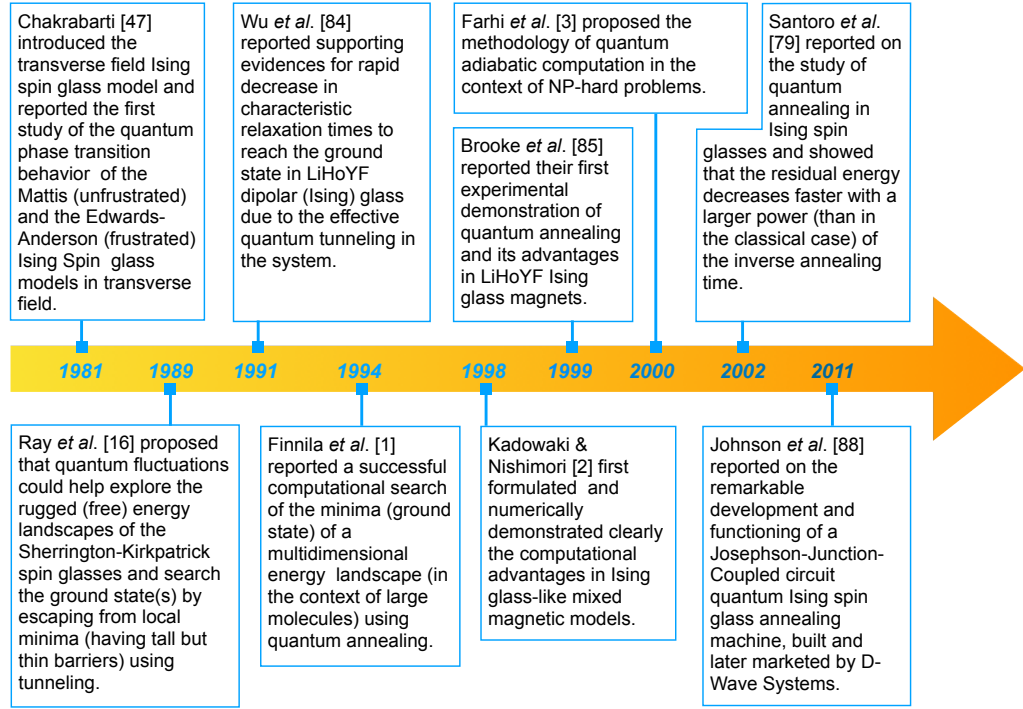


Figure 2. A brief Time-line for the development of Quantum Annealing.

is given by the ground state of the transverse field, in which all spins are aligned along the x axis of spin. This is a disordered state where the ground-state averaged magnetization in the z direction of spin is zero, i.e., $\langle \sigma_i^z \rangle = 0$. The targeted ground state of the Ising Hamiltonian for $\Gamma = 0$, however, is an ordered state in the sense that it has a fixed magnetization $+1$ or -1 for each σ_j^z . This implies that the system encounters a QPT during QA. Indeed, the model in Eq. (1.2) has QPTs at $\Gamma/J = \pm 1$. The finite size scaling of the energy gap at QPT depends on the character of the associated QPT, and the latter is determined by the property of the Ising Hamiltonian.

The character of a conventional continuous QPT is specified by critical exponents [20–23]. The size scaling of the energy gap at a quantum critical point is given as $\Delta_c \sim L^{-z}$ where L denotes the linear size of the system and the exponent z , known as the dynamical exponent, characterizes the associated quantum critical point (QCP). Therefore the time for QA to work scales polynomially with the system size. However, apart from this simple situation, the polynomial scaling of the energy gap at QPT is not always true. In fact, a discontinuous QPT usually gives rise to an exponential scaling with the system size. This can be understood phenomenologically as follows. Consider a quantum many-body system and focus on the two lowest energy levels. We assume that higher energy levels are highly separated from them. The effective Hamiltonian is then written as

$$H = \begin{bmatrix} \varepsilon_A & \Delta \\ \Delta & \varepsilon_B \end{bmatrix},$$

where ε_A and ε_B corresponds to the energies of the two local minima, and Δ denotes the tunneling energy between these two states. Figure 3 shows the energy levels of this Hamiltonian schematically. The discontinuous QPT corresponds to the change of the lowest energy level between A and B . The transition takes place where the bare energies ε_A and ε_B of two levels are degenerate. The energy gap at the transition is given by the twice of the tunneling energy Δ , and Δ is given by an exponential of the Hamming distance between the states A and B . Note

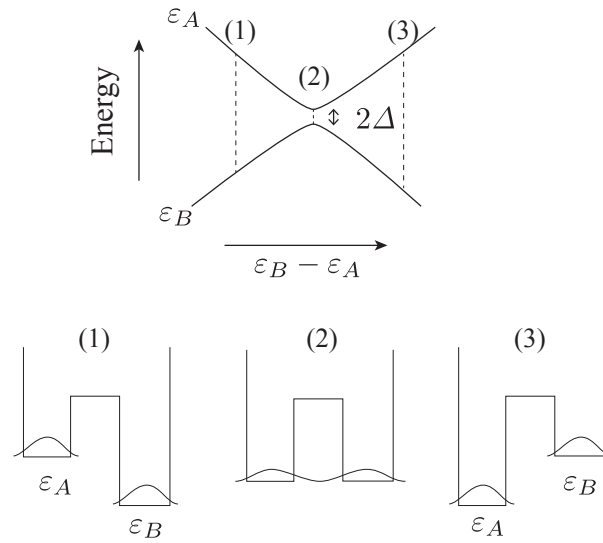


Figure 3. Schematic picture for an interchange of two energy levels. ε_A and ε_B corresponds to the energies of the two local minima. (1), (2), and (3) shows the situations with $\varepsilon_A \gg \varepsilon_B$, $\varepsilon_A = \varepsilon_B$, and $\varepsilon_A \ll \varepsilon_B$, respectively. In the case (2) with $\varepsilon_A = \varepsilon_B$, the energy gap is given by the twice of the tunneling energy Δ between the states A and B .

that the Hamming distance is the number of sites at which the spin orientation along z axis is different. Usually this distance increases linearly with the system size. Therefore the energy gap at a transition decays exponentially with the system size. Since the discontinuous QPT hinders QA, several ways to avoid the discontinuous QPT have been proposed. We will mention some of them in Sec. 4.

QA across a QPT is closely related to the Kibble-Zurek mechanism of defect generation following an annealing across a QCP. [24–30]. The system starting from the initial disordered ground state evolves adiabatically as far as the characteristic time of the instantaneous ground state (i.e., the inverse of the gap) is shorter than the annealing speed. However, on approaching a QPT, the characteristic time grows and hence the dynamics becomes non-adiabatic in the vicinity of the QCP. The state of the system after the passage through the QCP is no longer the ground state, rather a state with topological defects. The residual energy density, ε_{res} , i.e., the excess energy over the expected final ground state at the end of the QA is a monotonically decreasing function of the annealing duration τ . In case of a linear annealing through a conventional continuous QPT in a d -dimensional many-body system with the critical exponent ν for the correlation length and the dynamical exponent z , Kibble-Zurek scaling of the residual energy is given by $\varepsilon_{\text{res}} \sim \tau^{-d\nu/(z\nu+1)}$ as far as the system after annealing is in a gapped phase. The scaling of the residual energy density is modified from the Kibble-Zurek scaling for other unconventional continuous QPTs or discontinuous QPTs and when the annealing protocol involves a non-linear variation of the tuning parameter [30–32]. The scaling of the residual energy together with the scaling of the energy gap at QPT is an important measure that characterizes the property of QA [33,34].

(b) Transverse Ising models

Assuming the transverse field Hamiltonian as H_D , the total Hamiltonian of QA forms the transverse Ising models (TIMs). We briefly review properties of some representative TIMs in this subsection [24–27].

(i) Pure and disordered transverse Ising chain

As the simplest case we first consider the pure ferromagnetic one-dimensional TIM (1dTIM) given by Eq. (1.2). There are two phases of the ground state in this model separated by a quantum phase transition at $\Gamma/J = 1$. The ground state is disordered for $\Gamma/J > 1$, while it is ferromagnetically ordered for $\Gamma/J < 1$. At the critical point $\Gamma/J = 1$, the energy gap above the ground level vanishes as the system size $L \rightarrow \infty$. The scaling of the energy gap with the linear size L at the critical point is given by $\Delta \sim L^{-1}$. Critical exponents of the correlation length and the dynamical exponent are $\nu = 1$ and $z = 1$, respectively.

The scaling of the defect density following a QA of the pure 1dTIM was solved exactly by Dziarmaga [35]. Let us assume $\Gamma = -tJ/\tau$ with the parameter τ which denotes the inverse of the annealing speed. Using the periodic boundary condition in Eq. (1.2), and applying the Jordan-Wigner transformation followed by the Fourier transformation, the quantum time evolution of the spin state is reduced to decoupled Landau-Zener models of two-level systems for each momentum mode [22,23]. When the time t is varied from $-\infty$ to 0, with the initial state chosen to be the ground state of the initial Hamiltonian, the residual energy per spin at the final time $t = 0$ is found to be of the form

$$\varepsilon_{\text{res}} = \frac{1}{\pi} \frac{1}{\sqrt{2J\tau/\hbar}} \quad (1.4)$$

in the thermodynamic limit $L \rightarrow \infty$. We recall that the residual energy is defined as the excess energy that is the difference of the energy expectation value of $H(t=0)$ with respect to the evolved state at $t = 0$ from the ground energy of $H(t=0)$. According to the Kibble-Zurek scaling with $\nu = z = 1$, one has $\varepsilon_{\text{res}} \sim \tau^{-1/2}$ consistent with Eq. (1.4).

The disordered version of 1dTIM is given by

$$H = - \sum_j J_j \sigma_j^z \sigma_{j+1}^z - \Gamma \sum_j h_j \sigma_j^x, \quad (1.5)$$

where J_j is a random ferromagnetic coupling and h_i is a random transverse field obeying distributions $\pi_J(J)$ and $\pi_h(h)$, respectively. The phase transition of this model happens when $[\log J]_{\text{av}} = \log \Gamma + [\log h]_{\text{av}}$, where $[\dots]_{\text{av}}$ denotes the random average. The ground state is ferromagnetically ordered for $\Gamma < \exp([\log J]_{\text{av}} - [\log h]_{\text{av}})$, and disordered for $\Gamma > \exp([\log J]_{\text{av}} - [\log h]_{\text{av}})$ [36–39]. The phase transition is characterized by the infinite randomness fixed point, where the dimensionless parameter appearing in the distribution of the energy gap Δ is $(-\log \Delta)/\sqrt{L}$, implying that the energy gap scales as $e^{-C\sqrt{L}}$, where C is a positive constant. Therefore, even though the ground state of this model with $\Gamma = 0$ is trivial, the dynamics of QA to this state across the quantum phase transition is highly nontrivial. The size scaling of the typical gap suggests that the time to arrive at the target state by QA scales as subexponential with L . In connection to the Kibble-Zurek scaling, Dziarmaga and Caneva et al., reported that the density of kinks produced after QA scales as

$$[\rho_{\text{kink}}]_{\text{av}} \sim 1/\log^2 \alpha \tau \quad (1.6)$$

with an $\mathcal{O}(1)$ constant α [40,41]. Thus, the defect density decays in a logarithmically slow fashion with the annealing time τ which we reiterate makes QA difficult. However, it has been reported that SA for the one-dimensional disordered Ising model (i.e., Eq. (1.5) with $\Gamma = 0$) yields $[\rho_{\text{kink}}]_{\text{av}} \sim 1/\log \alpha' \tau$, where α' is a constant, which decays slower than Eq. (1.6) [42]. Therefore, this model reveals an evident advantage of QA over SA.

(ii) Pure transverse Ising model in higher dimensions

The two-dimensional TIM (2dTIM) may be the simplest model next to 1dTIM, though unlike the 1d case, the 2d model is not integrable. The equilibrium properties of the 2dTIM has been studied numerically and some of thermodynamic properties including the character of quantum and thermal phase transitions are available. Recently Schmitt et al., carried out numerical study of QA in 2dTIM in the context of the Kibble-Zurek scaling using state-of-the-art numerical methods

[43]. Their results are consistent with the Kibble-Zurek prediction. Study of out-of-equilibrium dynamics of a two-dimensional quantum system will be a direction of study in the near future.

The situation becomes simpler in the infinite dimension. The pure TIM in the infinite dimension is written as

$$H = -\frac{J}{N} \sum_{j < k} \sigma_j^z \sigma_k^z - \Gamma \sum_j \sigma_j^x, \quad (1.7)$$

where N denotes the number of spins. Note that each spin interacts with all the other spins with an equal strength. Defining the total spin operator as $\vec{S} = (1/2) \sum_{j=1}^N \vec{\sigma}_j$, this Hamiltonian can be arranged into

$$H = -2\frac{J}{N} S_z^2 - 2\Gamma S_x + \frac{J}{2}. \quad (1.8)$$

In the thermodynamic limit, this model undergoes a continuous QPT at $\Gamma = J$. The energy gap above the ground state behaves as $\Delta [(\Gamma - J)\Gamma]^{1/2}$ for $\Gamma \geq J$ and the size scaling of the energy gap at $\Gamma = 1$ is $\Delta_c \sim N^{-1/3}$ [44]. Introducing the effective dimension d_{eff} so that the system size N is tied to the linear size L by $L^{d_{\text{eff}}} = N$, one has relations between critical exponents as $z\nu = 1/2$ and $z/d_{\text{eff}} = 1/3$. Then, assuming $z = 1$ as in pure TIMs with finite dimension, one obtains $\nu = 1/2$ and $d_{\text{eff}} = 3$. Caneva et al., studied QA of the present model and obtained $\varepsilon_{\text{res}} \sim \tau^{-1/3}$. This scaling is inconsistent with the Kibble-Zurek scaling, since the latter predicts τ^{-1} . Acevedo et al., revealed that there is an anomaly in the transition amplitude between the ground and excited states in the present model [45]. Therefore the naive phenomenological argument to derive the Kibble-Zurek scaling does not apply to the system in infinite dimension. We shall also discuss an extension of the Hamiltonian (1.7) to the p -body interacting model in Sec. 4 and argue that the QA does not work in this model with odd p .

(iii) Transverse Ising spin glass

The Hamiltonian of the Edwards-Anderson [46] version of the transverse Ising spin glass, introduced by Chakrabarti in 1981 [47], is written as

$$H = - \sum_{\langle jk \rangle} J_{jk} \sigma_j^z \sigma_k^z - \Gamma \sum_j \sigma_j^x, \quad (1.9)$$

where $\langle jk \rangle$ stands for nearest neighbour pairs and J_{jk} are independent random variables. The order parameter of a spin glass is defined in terms of the spin overlap between different replicas. Supposing that $\sigma_j^{\alpha,a}$ denotes the spin operator for a replicated system labeled by a , the overlap operator between replicas $a = 1$ and $a = 2$ is defined by $R_{1,2} = (1/N) \sum_{i=1}^N \sigma_j^{z,1} \sigma_j^{z,2}$. The order parameter is then given by $q = [\langle R_{1,2} \rangle]_{\text{av}}$. The spin glass order is characterized by $q > 0$ with zero magnetization $m = 0$, where the magnetization is defined by $m = [\langle (1/N) \sum_{i=1}^N \sigma_j^z \rangle]_{\text{av}}$. This means that the spin configuration is spatially random but frozen. Rieger et al., and Guo et al., investigated the character of QPTs of this model with the Gaussian distribution of J_{jk} with zero mean and unit variance in square and cubic lattices, respectively, by means of the quantum Monte Carlo simulation [48,49]. Singh and Young studied $\pm J$ model where J_{kj} takes +1 or -1 with equal probability for dimensions up to $d = 8$ using the linked cluster expansion to determine the location of the QCP [50]. Subsequently, QPTs of these models were reconsidered by Miyazaki and Nishimori [51] and by Matoz-Fernandez and Romá [52] using the real-space renormalization group and the quantum Monte-Carlo with parallel-tempering, respectively. They concluded that the QPTs in transverse Ising spin glasses in two and three dimensions were compatible with the infinite randomness fixed point with the critical exponents ν and ψ , where ψ specifies the activation type of size scaling of the energy gap as $[\log \Delta]_{\text{av}} \sim N^{\psi/d}$ [53–57]. The estimated exponents for the Gaussian model were $\nu \approx 1.2$ and $\psi \approx 0.44$ in two dimension [51,52] and $\nu \approx 0.94$ in three dimension [51].

The Hamiltonian of the transverse Ising spin glass in infinite dimension, i.e., the quantum Sherrington-Kirkpatrick (SK) model, is written as [16]

$$H = -\frac{1}{\sqrt{N}} \sum_{1 \leq j < k \leq N} J_{jk} \sigma_j^z \sigma_k^z - \Gamma \sum_{j=1}^N \sigma_j^x, \quad (1.10)$$

The classical SK model in the absence of the transverse field unveiled the existence of so-called replica symmetry breaking (RSB) in the spin glass phase [58,59], where the overlap $R_{1,2}$ has a dispersed continuous distribution in the thermodynamic limit. Ray et al., conjectured on the basis of the quantum Monte-Carlo simulation the collapse of a continuous distribution for the classical SK model into a delta function in the presence of any amount of the transverse field [16], which paved the way for using quantum tunneling in finding the global minimum or ground state of SK spin glass model. In the classical model, due to random interactions between spins at different lattice sites, such systems have many local minima in free energy which are separated by large energy barriers of order $O(N)$, where N is the system size [59]. This induces non-ergodicity in the system and eventually breaks the replica symmetry of the system. As a result, finding the ground state or global minimum of such systems is a very hard problem; for SK spin glass model, it turns out to be NP (non-deterministic polynomial-time) hard. The system indeed gets trapped into one of the local minima inside the spin glass phase, due to the highly rugged nature of free-energy landscape. This leads to a broad order parameter distribution in the spin glass phase [58]. In addition to a peak value of the order parameter distribution, it is extended up to the zero value of the order parameter even in the thermodynamic limit.

It seems that the scenario may change drastically, when a transverse field is applied on the SK spin glass [16]. The presence of quantum fluctuations induces ergodicity in the system, since quantum tunneling becomes possible between the local minima separated by tall and narrow free-energy barriers. This indicates the restoration of replica symmetry breaking for quantum SK spin glass model. As a result, the order parameter distribution should be sharply peaked at a point for quantum SK model in the thermodynamic limit. This ergodic behavior of quantum SK model is responsible for advantage in quantum annealing in comparison to simulated annealing.

This conjecture was criticized by Young [60] by solving numerically the effective one-dimensional model to which the quantum SK model can be mapped in the $N \rightarrow \infty$ limit; this work predicted that the replica symmetric solution is unstable down to zero temperature. On the contrary, Mukherjee et al., [61] explored the behavior of the order parameter distribution of the quantum SK model in the spin glass phase using Monte Carlo technique for the effective Suzuki-Trotter Hamiltonian at finite temperatures (see Eq. (2.1) discussed later) and the exact diagonalization method at zero temperature. It has been found that there exists a low temperature regime in the spin glass phase, where the order parameter distribution becomes peaked around its most probable value in thermodynamic limit, thus suggesting the ergodic behavior. On the other hand, the order parameter distribution remains Parisi type in high temperature regime, which indicates the non-ergodic behavior of the system in this part of the spin glass phase. These two regions of the spin glass phase are separated by a boundary, connecting the zero temperature-zero transverse field point and the quantum-classical crossover point on the phase boundary [61,62]. In addition, quantum annealing has also been investigated for quantum SK model using Suzuki-Trotter Hamiltonian dynamics in both the ergodic and non-ergodic regimes. The average annealing time was estimated, when both the temperature and the transverse-field were annealed down to some fixed low values, starting from the paramagnetic phase. It was found that the average annealing time is independent of the system size, when the annealing is performed through the ergodic (quantum fluctuation dominated) region, whereas it grows strongly with the system size, when the annealing is carried out through the non-ergodic (classical fluctuation dominated) region. This suggests that the quantum annealing has potential to detect whether a phase is ergodic or non-ergodic. Also, the average annealing time to approach a same ground state is small for annealing through ergodic regime compared to that through the non-ergodic regime. The QA for SK spin glass is also studied by tuning both transverse and

longitudinal fields, and it has been shown that this protocol exhibits some effectiveness compared to the QA by varying the transverse field only [63].

Recently, Leschke et al., proved rigorously nonzero variance of the overlap in the thermodynamic limit of the quantum SK model at sufficiently low temperature with small but finite transverse field [64]. Their study reveals a dispersed distribution of the overlap, therefore the existence of RSB. However the controversy about the continuous distribution of the overlap in the quantum SK model is still an open problem [65].

(c) Transverse Ising model for satisfiability

The satisfiability problem is known as one of the basic combinatorial optimization problem in computer science. Given the number of bits and constraints among bits, the problem is to determine whether the bit configuration satisfying all the constraints exists or not. In the case of 3-satisfiability problems, or 3-SATs in short, each constraint involves three bits drawn randomly. Using the spin language, a constraint for three spins S_i , S_j and S_k taking the values ± 1 can be represented as $(S_i + S_j + S_k - 1)^2$, for instance. This vanishes and is called satisfied when two of the three spins are $+1$ and the other spin is -1 , otherwise it gives a nonzero and positive value. The Exact Cover, a variant of the 3-SAT, consists of M such constraints for N spins, and thus the corresponding quantum model that needs to be annealed is given by

$$H = \sum_{m=1}^M (\sigma_{i_m}^z + \sigma_{j_m}^z + \sigma_{k_m}^z - 1)^2 - \Gamma \sum_{j=1}^N \sigma_j^x. \quad (1.11)$$

If one arrives at the exact ground state for $\Gamma = 0$, by annealing the field Γ , then one can solve the Exact Cover. However, the Exact Cover is an NP-complete problem which no known algorithm can solve in a time polynomial in N . Young et al., studied Eq. (1.11) by means of the quantum Monte-Carlo method [66]. They found that some instances of the model show a discontinuous first-order QPT with an exponentially small energy gap and the fraction of such instances grows toward unity with increasing N . Jörg et al. also reported occurrence of a first-order QPT in the random 3-XORSAT problem, which is another variant of the 3-SAT [67].

2. Implementation of quantum annealing

Implementing QA is a challenging task, since one needs to evolve a many-spin state under a quantum many-body Hamiltonian. In this section, we review results from numerical simulation using real-time dynamics as well as Monte-Carlo dynamics, and from quantum simulations using hardwares.

(a) Results from numerical simulation for real time dynamics

The real-time evolution of a quantum system governed by the Schrödinger equation can be computed in general by solving a linear differential equation. However, since the number of unknown functions of time increases as 2^N with the number of spins, the system size acceptable to a conventional computer is limited to $N \sim O(10)$. Kadowaki and Nishimori reported in the seminal paper that QA yields better solutions than the classical simulated annealing on the basis of their simulation for 8 spin systems of a frustrated model and the SK model [2]. Farhi et al., reported the numerical result for the Exact Cover problem with the number of spins up to 20 [3]. Exact Cover is one of the NP-complete problems, which no known classical algorithm can solve in a time polynomial in the number of spins. The numerical result suggested a quadratic scaling of the runtime in QA with respect to the number of spins. However, this scaling should turn into an exponential one for larger size as shown by the quantum Monte-Carlo study for the energy gap [66].

Restricted to systems in one dimension, there are efficient methods of numerical simulation for real-time evolution. In case of 1dTIMs without the longitudinal field, irrespective of disorder,

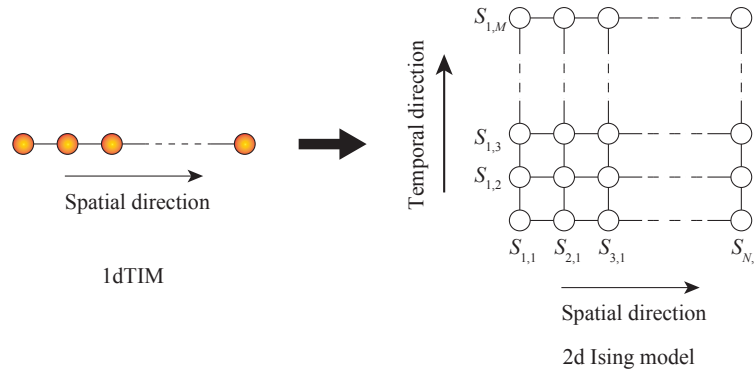


Figure 4. Schematic picture of the Suzuki-Trotter mapping. A 1dTIM is mapped to a two-dimensional classical Ising model on the square lattice. The additional dimension corresponds to the time. $S_{j,m}$ denotes an Ising-spin variable at spatial site j and temporal site m .

the Schrödinger equation of the spin state reduces to the Bogoliubov-de Gennes equation of $2N$ unknown functions of time through the Jordan-Wigner's fermionization and the Bogoliubov transformation [68]. Generic 1dTIMs with longitudinal fields cannot be mapped to free fermion models. However, time evolution of generic 1dTIMs can be simulated using the time-dependent density matrix renormalization group (tDMRG) proposed by White and feiguin [69] or the time evolving block decimation (TEBD) by Vidal [70]. In addition, the infinite system of 1dTIMs with no disorder can be simulated using an infinite method of TEBD (iTEBD) [71]. These methods serve the study of QA in 1dTIM with a uniform or disordered longitudinal field [72,73].

(b) Results from numerical simulation for Monte-Carlo dynamics

A d -dimensional TIM in finite temperature (denoted by β^{-1}) with spin-spin coupling J_{jk} and transverse field Γ can be mapped to a $(d+1)$ -dimensional classical Ising model by the Suzuki-Trotter mapping [74,75]. The resulting Hamiltonian H_{eff} is given by

$$H_{\text{eff}} = - \sum_{m=1}^M \sum_{j < k} \frac{J_{jk}}{M} S_{j,m} S_{k,m} - \frac{M}{2\beta} \log \coth \frac{\beta\Gamma}{M} \sum_{j=1}^N \sum_{m=1}^M S_{j,m} S_{j,m+1}, \quad (2.1)$$

where β is the inverse temperature, M is the Trotter number, $S_{j,m}$ denotes the spin variable with the spatial site j and temporal site m taking values ± 1 , and we defined the sign of J_{jk} according to Eq. (1.9). In Figure 4, we schematically illustrate the mapping of 1dTIM into a (1+1)-dimensional classical Ising model. One can simulate in principle any TIM in and out of equilibrium using this effective Hamiltonian and the Monte-Carlo method. This method is called the quantum Monte-Carlo method (QMC). Although the number β/M controls the accuracy of QMC, the cluster-update method invented by Swendsen and Wang along the temporal direction enables to have $\beta/M \rightarrow 0$ [76,77]. QMC is known to give rise to the sign problem and fail when the model involves the frustration. However, QMC for TIM is free from the sign problem. Therefore QMC is a powerful method of classical computation in simulating TIM.

QA can be implemented in QMC by regarding the Monte-Carlo step as time. The dynamics realized by QMC is not the quantum dynamics governed by the Schrödinger equation but the stochastic one. However, QA with QMC serves the purpose of solving an optimization problem using a classical computer [78]. Several works have shown so far that QA with QMC works in variety of optimization problems, such as two-dimensional Ising spin glass [79,80], travelling salesman problem [81], and 3-SATs [82]. Figure 5 shows comparison between QA by QMC and

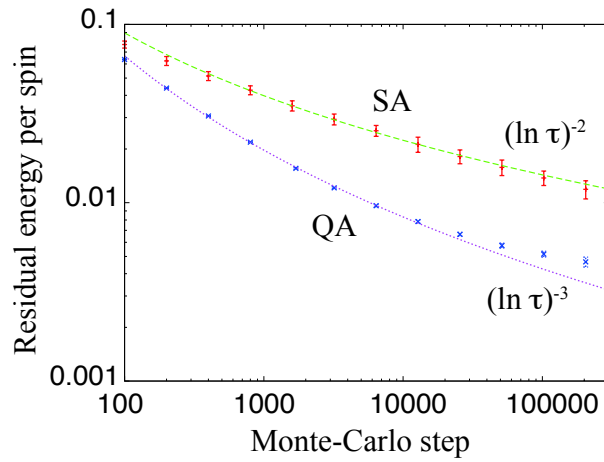


Figure 5. Comparison of the residual energy between QA by QMC and SA for the two-dimensional spin glass model with 99×99 spins with random coupling J_{jk} from the uniform distribution between -2 and 2. The cluster-flip algorithm in the imaginary-time direction was used in QMC. SA was started from the initial temperature $T = 5.0$, while QA was from $\Gamma = 5.0$ with $T = 0.01$. The average was taken over 100 runs for a single instance in SA, and for 16 instances in QA. The decay of the residual energy in SA is well fitted by $(\log \tau)^{-2}$. As for QA, it is approximated by $(\log \tau)^{-3}$, except for long annealing time where the decay rate is smaller. (Taken from ref. [83].)

SA in the two-dimensional spin glass model [83]. This result implies outperformance of QA over SA. Although an opposite result has been reported for harder 3-SAT problems [82], numerical studies using QMC suggest that there are problems for which QA is potentially advantageous over SA due to the restoration of ergodicity by quantum fluctuation [16].

(c) Results from quantum simulation using hardware

The most efficient way to perform QA is use a quantum magnetic material which realizes a TIM with a temporally controllable transverse field. $\text{LiHo}_x\text{Y}_{1-x}\text{F}_4$ is a material that models a disordered Ising model and it also realizes a disordered TIM by application of the magnetic field perpendicular to the easy axis of magnetization [84]. Brooke et al., investigated two protocols, QA and thermal annealing (TA), using this material with $x = 0.44$. In QA, the transverse field Γ was strengthened at high temperature, the system was cooled, and then Γ is weakened to Γ_f at low temperature. On the other hand, in TA, the temperature was lowered with keeping $\Gamma = 0$, and then Γ was raised to Γ_f . In both protocols, the initial and final sets of Γ and temperature were the same and the durations were the same as well. The ground state at Γ_f as the target state is a glassy ferromagnetic state. Brooke et al., reported that the state after QA much is closer to an equilibrium state than the state after TA [85]. This result implies that QA brings the state to the target faster than TA. Quite recently Säubert et al., studied QA and TA of the same material and detailed the dynamical behavior of the energy landscape during QA. They showed that the transverse field applied in QA induced random longitudinal fields, implying that the energy landscape of the problem Hamiltonian H_P evolved as QA proceeded [86]. This evolving landscape may be an issue of future work related to QA.

Progress in Rydberg atom experiments enables to use Rydberg atoms as a quantum simulator. Keesling et al., performed a quantum simulation of a sort of QA using an array of 51 Rydberg atoms. In this simulation, the system is described by the many-body Hamiltonian $H = (\Omega/2) \sum_i (|g_i\rangle\langle r_i| + h.c.) - \Delta \sum_i n_i + \sum_{j < k} V_{jk} n_j n_k$, where $|g_j\rangle$ and $|r_j\rangle$ denote the ground and the excited Rydberg states, respectively, of atoms, $n_j = |r_j\rangle\langle r_j|$, and V_{jk} is the van der Waals

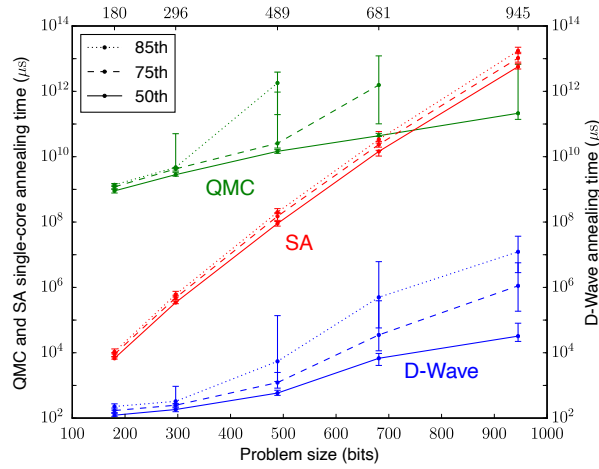


Figure 6. Comparison of the time to reach the ground state with 99% success probability as a function of the problem size in D-Wave 2X, simulated annealing (SA), and quantum Monte-Carlo (QMC). The runtime in SA and QMC is defined by $n_{\text{sweeps}}NT_{\text{update}}$, where n_{sweeps} is the number of sweeps (one sweep attempts to update all spins). T_{update} is the single-spin update time for SA and the update time of a spin-cluster along the temporal direction. It is set as $T_{\text{update}} = 1/5$ ns for SA and 10×870 ns for QMC. Data for 50th, 75th, and 85th percentile taken from a set of 100 instances are shown. The error bars represent 95% confidence interval from bootstrapping. Taken from ref. [89].

interaction with the strength which decays as $1/|j - k|^6$. The model exhibits a QPT, achieved by tuning the parameter Δ , belonging to the same universality class as that of 1dTIM. Keesling et al., observed that the Kibble-Zurek scaling for the kink density arising due to the sweeping of the parameter Δ , turns out to be the very same as that in 1dTIM [87].

In order to apply QA as a computation to an optimization problem in practice, spin-spin interactions and longitudinal fields in addition to the transverse field need to be locally controllable. A Canadian venture company, D-Wave Systems, has developed a quantum annealing machine named as a quantum annealer, which consists of programmable coupled superconducting flux qubits and performs QA to various Ising models [88]. The number of qubits in the latest machine is beyond five thousands. This is 100 times larger than the number of qubits in the current gate-based quantum computer. Denchev et al., benchmarked D-Wave 2X using 100 instances of the weak-strong cluster model with up to 945 spins [89]. Qubits in D-Wave 2X form the so-called chimera graph with unit cells consisting of 8 qubits. In the weak-strong cluster model, there are all-all ferromagnetic couplings inside the cell, and half of the spins in a cell ferromagnetically couple with those in neighboring cells. In addition, weak longitudinal fields are applied to spins in randomly chosen cell, while strong fields anti-parallel to the weak ones are applied to spins in the other cells. Figure 6 shows the time to reach the ground state with 99% success probability. For D-Wave, this time is defined by $20 \mu\text{s} [\log(1 - 0.99)/\log(1 - p)]$ for an instance, where the annealing time is fixed at $20 \mu\text{s}$ and p denotes the success probability to obtain the ground state estimated from many runs. As for SA and QMC, it is the runtime on a single processor. Regarding the median from 100 instances, D-Wave 2X is 10^8 and 10^7 times faster than SA and QMC, respectively.

Boixo et al., tested D-Wave's quantum annealer to a spin glass model $H_P = -\sum_{\langle jk \rangle} J_{jk} \sigma_j^z \sigma_k^z$, where J_{jk} is chosen randomly from $J = \pm 1$, with $N = 108$ spins and reported that the results of quantum annealer correlated well with those obtained by QA with QMC [90]. Figure 7 shows the comparison of the histogram of the success probability between D-Wave's quantum annealer (DW) and QA with QMC (named as Simulated QA). The bimodal distribution which is common in D-Wave and QMC could be an evidence that the system embedded in D-Wave's quantum

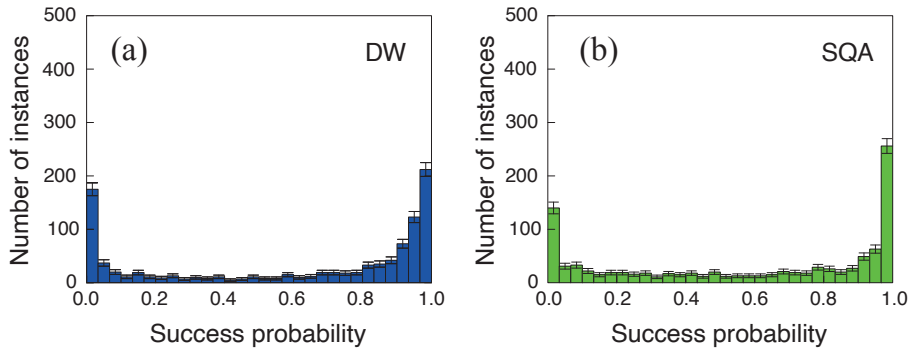


Figure 7. Comparison of the histogram of the probability of finding the ground state between D-Wave One and QA with QMC (simulated QA) over 1000 instances of the spin glass model with $N = 108$ spins. Taken from ref. [90].

annealer was a quantum system. However, Shin et al., reported that the classical spin vector model along with the Monte-Carlo dynamics, named as the spin vector Monte-Carlo (SVMC) model, provided as strong correlation with D-Wave's data as QMC [91]. The classical spin vector model is represented by the Hamiltonian

$$H(t) = -A(t) \sum_{j=1}^N \cos \theta_j - B(t) \sum_{\langle jk \rangle} J_{jk} \sin \theta_j \sin \theta_k, \quad (2.2)$$

where θ_j denotes the angle of the unit vector at site j in the xz plane. These works have raised a problem to identify the model of D-Wave's quantum annealer [92]. Bando et al., studied the Kibble-Zurek scaling in 1dTIM using D-Wave 2000Q and found that the kink density defined by $n = (1/2N) \sum_{j=1}^N (1 - \langle \sigma_j^z \sigma_{j+1}^z \rangle) = \varepsilon_{\text{res}}/2$ scaled with the annealing time t_a as $n \sim t_a^{-\alpha}$ with $\alpha \approx 0.20$ by the device at NASA and $\alpha \approx 0.34$ by the one at D-Wave Systems [93]. As mentioned in Sec. i, the scaling of the kink density is predicted as $n \sim t_a^{-1/2}$ for an isolated system belonging to one-dimensional Ising universality class. The authors in ref. [93] compared numerical simulations for 1dTIM with coupling to an environment and for SVMC with the experiment, and concluded that the quantum model agreed better with the experiment. Recently, King et al., studied QA of 1dTIM using D-Wave 2000Q [73], focusing on shorter annealing times than those in the previous works. For short annealing times, the system in the device is less affected by environment as we shall discuss in the next section. Comparing analytic and numerical computation for the Schrödinger dynamics of the isolated 1dTIM, the QMC simulation, and the SVMC simulation with the experiment by D-Wave 2000Q, King et al., reported that only the Schrödinger dynamics of the isolated 1dTIM with a small amount of disorder can explain all the experimental results [73]. Also, in ref. [94], fully connected Sherrington-Kirkpatrick model with random couplings was programmed using D-Wave TwoTM annealer, where optimal parameter setting allowed better performance of the quantum annealer when compared to those obtained using optimized simulated annealing algorithms.

3. Effects of environment on QA

Although QA is ideally performed in an isolated system, any real system is always coupled to an environment and hence susceptible to decoherence. In fact, the system in D-Wave's device is believed to be affected considerably by an environment when the annealing time is longer than a few μs . Therefore it is very important to study an effect of environment in QA.

There is a variety of models representing an environment. Caldeira and Leggett, in their seminal work analyzed the dynamics of flux state in a SQUID and constructed a simple model of

a two-level system coupled to a boson bath, where bosons are attributed to the electro-magnetic field coming from the fluctuating current [95]. Leggett et al., elaborated on the single-spin model coupled a boson bath [96]. Thus, considering QA performed with superconducting flux qubits, the model which includes the effect of an environment should be an extension of the Caldeira-Leggett model to many spins. Hamiltonian is written as $H(t) = H_S(t) + H_B + H_{\text{int}}$, where the system Hamiltonian $H_S(t)$ is given by Eq. (1.1). The bath is represented by the collection of harmonic oscillators. Hence the bath Hamiltonian H_B is given, using the boson operators $b_{j,a}$ and $b_{j,a}^\dagger$ for site j and mode a , by

$$H_B = \sum_{j,a} \hbar \omega_a b_{j,a}^\dagger b_{j,a}, \quad (3.1)$$

where ω_a is the frequency of the harmonic oscillator of mode a . H_{int} represents the interaction between the system and the bath, and written as

$$H_{\text{int}} = \sum_{j=1}^N (\sigma_j^x Q_j^x + \sigma_j^z Q_j^z) \quad (3.2)$$

where Q_j^γ ($\gamma = x, z$) is the bath operators given by $Q_j^\gamma = \sum_a \lambda_a^\gamma (b_{j,a}^\dagger + b_{j,a})$. The spectral density of the boson bath is assumed as $J_\gamma(\omega) = \sum_a (\lambda_a^\gamma)^2 \delta(\omega - \omega_a) = \eta_\gamma \omega^s e^{-\omega/\omega_c}$, where η_γ denotes the coupling strength of the system-bath interaction and ω_c is the energy cutoff of the bath spectrum. The Ohmic bath refers to $s = 1$, while the super-Ohmic and sub-Ohmic baths refer to $s > 1$ and $s < 1$, respectively.

Let us now move to study the time evolution assuming that the state of the composite system is described by the density operator $\rho(t)$ at the instant t . The initial state is assumed to be a direct product state of the form $\rho(0) = |\psi(0)\rangle\langle\psi(0)| \otimes e^{-H_B/T} / Z_B$, where $|\psi(0)\rangle$ denotes a state vector of the system, T is the temperature, and Z_B is the partition function of the bath. Since we are interested in the behavior of the system, we consider the reduced density operator describing the system, $\rho_S(t) = \text{Tr}_B \rho(t)$, where Tr_B stands for the trace with respect to the bosonic degrees of freedom.

Amin explored the success probability of QA for a range of annealing time t_a obtained by solving numerically the quantum Redfield master equation for an instance of 16 spins of random Ising model in a random longitudinal field with nonzero η_z and $\eta_x = 0$ [97]. The obtained success probability is a nonmonotonic function of t_a . For short t_a , the spin system is not influenced by the bath and hence the success probability increases with increasing t_a . In a middle range of t_a , the thermal environment disturbs the system's adiabatic evolution more for longer t_a , hence leading to decreasing success probability. For very long t_a , finally, the system evolves keeping the thermal equilibrium with the bath until it is frozen near the end of QA. The freezing happens because $H_S(t_a)$ and H_{int} are commutable when $\eta_x = 0$ and hence the relaxation time diverges as $t \rightarrow t_a$. Thus the success probability in this regime goes to the probability of the ground state at the thermal distribution as $t_a \rightarrow \infty$.

QA of 1dTIM in the presence of an environment has been attracted a lot of attention in the context of the Kibble-Zurek scaling. Assuming $Q_j^z = 0$, namely, the boson bath coupled to σ^x , 1dTIM with coupling to the boson bath is mapped to a noninteracting fermion model with a fermion-boson coupling through the Jordan-Wigner transformation. Then the problem is significantly tractable, compared to the situation with $\eta_z \neq 0$. Patané et al., studied the density of excitation following QA using the Keldish technique. Based on the ansatz that the density of excitation \mathcal{E} is given by the sum of the coherent part \mathcal{E}_{coh} and the incoherent part \mathcal{E}_{inc} due to the environment, Patané et al., obtained $\mathcal{E}_{\text{inc}} \sim \eta_x T^4 \tau$ for the Ohmic bath with temperature T when QA ends near the quantum critical point [98,99]. The incoherent part increases with τ in contrast to the coherent part, hence its scaling is called the anti-Kibble-Zurek scaling. Nalbach et al., studied the model with the spatially correlated bath where all spins are coupled to a single bath, i.e., $H_{\text{int}} = Q^x \sum_j \sigma_j^x$ and $H_B = \sum_a \hbar \omega_a b_a^\dagger b_a$ with $Q = \sum_a \lambda_a (b_a^\dagger + b_a)$. In this situation, the correlation length is the largest of the Kibble-Zurek length scale $\xi_{\text{KZ}} \sim \tau^{1/2}$ and the thermal

length scale $\xi_T \sim T^{-1}$. When $1 \ll \xi_T < \xi_{KZ}$, the thermal effect comes into play in the density of excitation. Thus, it is suggested that $\mathcal{E} \sim \eta T(\tau T^2) \sim \eta_x T^3 \tau$ for $\sqrt{\tau} \ll T \ll 1$ in this model. Nalbach et al., proposed this scaling relation and confirmed using the dissipative Landau-Zener theory for the two-level system [100]. Dutta et al., studied 1dTIM in the presence of a spatially homogeneous Gaussian white noise on the transverse field, instead of considering the coupling to a boson bath. This stochastic perturbation yields an effective dynamics of the noise-averaged density operator for an open quantum system. Then the noise-averaged density of excitation has an incoherent part which scales as $\mathcal{E}_{\text{inc}} \sim \tilde{\eta}_x \tau$, where $\tilde{\eta}_x$ is the strength of the noise [101]. Weinberg et al., studied a similar model but with a spatially uncorrelated and temporally correlated noise. The numerical result showed the same scaling as ref. [101]. Weinberg et al., also performed quantum simulation for 2dTIM using D-Wave 2000Q and obtained scaling for the residual energy $\varepsilon_{\text{res}} \sim a\tau^{-\alpha} + b\tau^\beta$ with $\alpha \approx 0.74$ and $\beta \approx 0.456$ [102]. The first term is consistent with the Kibble-Zurek scaling for 2dTIM with the exponent $d\nu/(z\nu + 1) \approx 0.77$, where $d = 2$, $z = 1$ and $\nu \approx 0.63$ [103]. Note that the scaling of the second term corresponding to the incoherent part is different from that in 1dTIM, implying that $\mathcal{E}_{\text{inc}} \sim \tau$ is specific to 1dTIM. The anti-Kibble Zurek mechanism in the presence of non-thermal bath has been also discussed in the framework of the Lindblad formalism in refs. [104–108]

The Kibble-Zurek and anti-Kibble-Zurek scalings implies the existence of a global or local minimum of the density of excitation. Based on the numerical study using the Redfield master equation in the momentum space for 1dTIM with the boson bath, Eqs. (3.1) and (3.2) with $Q_j^z = 0$, Arceci et al., identified the region in the $T - \eta_x$ -plane where there exists the local or global minimum of the density of defects after QA [109]. Interestingly, a global minimum of the density of defects appears in the digitized QA, in which the time-evolution operator inducing QA is split into slices with a finite time width and further split into those involving only H_D and those involving only H_P [110], suggesting that the decomposition of the time-evolution operator has an influence as a decoherence on the dynamics of a closed system.

Many studies of 1dTIM with a boson bath focusing on the Kibble-Zurek physics have assumed $Q_j^z = 0$, namely, coupling between the system operators σ_j^x and bosons. However, in experimental systems such as those made of coupled superconducting flux qubits, coupling between σ_j^z and Q_j^z is rather important [96]. Recently, Suzuki et al., developed new matrix-product-state-based methods for 1dTIM with a boson bath with $H_{\text{int}} = \sum_j Q_j^z \sigma_j^z$, which enables the simulation of finite pure and disordered systems with $O(10^2)$ spins [111,112] or an infinite translationally invariant system [113]. Using the infinite-system method, Oshiyama found modified Kibble-Zurek scaling in 1dTIM coupled to the bath at zero temperature [112]. Oshiyama et al., also studied QA of 1dTIM with the bath at finite temperatures. In the thermal environment at finite temperature T , the infinitely slow QA ($t_a \rightarrow \infty$) can be regarded as the quasistatic and isothermal process, hence the final energy should be identical to the thermal average of $B(t_a)H_P$ at T . When t_a is sufficiently long but finite, the energy of the system has an excess from the thermal average. Oshiyama et al., found and numerically confirmed that this excess energy scales with t_a as $t_a^{-1/3}$, for the linear annealing protocol [113].

4. Avoiding first-order phase transitions: Closed systems

As discussed in Sec. 1(a), it has been generally observed (with a few exceptions) that the minimum energy gap decreases exponentially with the system size for a first-order phase transition, whereas it shows a polynomial decrement in system size for a second-order phase transition. Therefore, the order of phase transitions is an important factor in determining the efficiency of the quantum annealing algorithm.

(a) Quantum ferromagnetic model

We consider here a ferromagnetic p -spin model in the transverse field. The Hamiltonian for such a system is given by

$$H = -N \left(\frac{1}{N} \sum_{i=1}^N \sigma_i^z \right)^p - \Gamma \sum_{i=1}^N \sigma_i^x, \quad (4.1)$$

where σ_i^z and σ_i^x are usual Pauli matrices at the lattice site i , Γ is the magnetic field in transverse direction and N is the number of spins and p is an integer. These type of models were initially introduced in the context of spin glasses. The ground state of the classical model at zero temperature with $\Gamma = 0$, corresponds to all spins aligned in the same direction. For even p , all the spins in up or down states are valid ground states, whereas odd p has a unique ground state when all the spins are in up states. Therefore, for simplicity, we will concentrate here on the odd p cases. For $p = 2$, the Hamiltonian in Eq. (4.1) reduces to an infinite-range Ising model which can be mapped to the usual mean field Curie-Weiss model exhibiting continuous phase transitions. On the other hand, for $p > 2$, both classical and quantum phase transitions of the system are discontinuous.

Using Suzuki-Trotter formalism and “static” approximation, the phase diagram of the p -spin ferromagnetic model can be found in $\Gamma - T$ plane for different values of p (see Fig. 8) [114]. In the limit of $p \rightarrow \infty$, using perturbation theory, the minimum energy gap of the system can be calculated as $\Delta_{\min} = 2N2^{-N/2}$ [114]. This indicates that the energy gap between the ground and excited states closes exponentially fast with the system size at the transition point. For a general p , an explicit form of the energy gap is not available so that one can comment about its scaling with the system size, however, the same scaling can be inferred from numerical calculations.

The energy gap of the system can be calculated numerically using two complementary methods as a function of the transverse-field Γ [114]. Using these numerical methods, we can find the transition point Γ_c where the energy gap shows a minima that scales with the system size. In the present case, the energy spectrum of the system has been studied for $3 \leq p \leq 31$. The Hamiltonian in Eq. (4.1) is represented by a sparse matrix of dimension 2^N . For such systems, Lanczos method provides nearly exact extreme eigenvalues of the Hamiltonian for the system size $N \leq 21$. From the results of the Lanczos method for $N \leq 21$, it has been found that the transition happens between two states with the maximum possible angular momentum $l = N/2$. The efficiency of the numerical simulation can be improved by exploiting the fact that the total angular momentum L^2 commutes with the Hamiltonian H in Eq. (4.1), (where L is the total angular momentum of N spins). Therefore the transition occurs mainly in the subspace of dimension $2l + 1 = N + 1$. In this subspace, the Hamiltonian assumes a tri-diagonal form and the resulting tri-diagonal matrix can be diagonalized efficiently for a system with size $N \sim 100$ in just a few seconds. The energy gap has been shown in the left panel of Fig. 9 as a function of Γ for $p = 3$ and different N . The gap becomes minimum at the critical value of Γ that agrees with analytically predicted value. One can observe that the region where the gap closes gets narrower as the value of N is increased. The minimum energy gap Δ_{\min} is further plotted as a function of N for different values of p to find its dependence on N (see right panel of Fig. 9). It has been found that the minimum energy gap decays exponentially as $\Delta_{\min} \propto N2^{-N\alpha}$ for $p \geq 3$. The minimum energy gap closes exponentially fast as expected for the first order phase transition. The value of exponent α can be computed numerically from the right panel of Fig. 9. These exponents are also calculated analytically using instantonic approach. A comparison of values of α for different values of p are given in Table 1 of Ref. [114].

Due to an exponential decay of energy gap with the system size, the running time increases exponentially for the case of a first-order phase transition, and thus reducing the efficiency of QA process. Therefore, it is an important issue to investigate whether one can avoid first-order phase transitions in the annealing path to solve the optimization problem efficiently using QA algorithm. Below we discuss various methods to speed up a quantum annealing process.

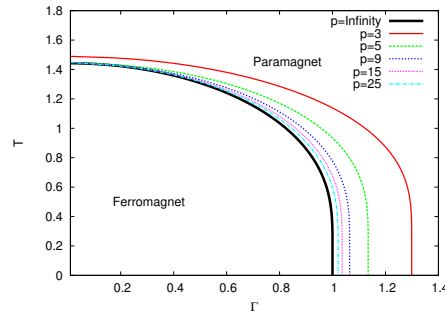


Figure 8. Phase diagram of the ferromagnetic p -spin model in the $T - \Gamma$ plane for different values of p . The ferromagnetic and quantum paramagnetic phases are separated by first-order phase transitions. Taken from [114].

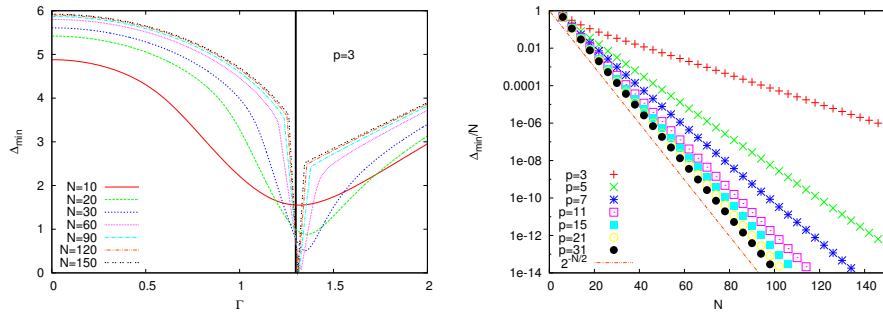


Figure 9. Left Panel: Variation of the energy gap as a function of Γ for $p = 3$ computed using an exact diagonalization method as described in the text. The gap vanishes exponentially fast with the system size N near the critical point Γ_c (the black vertical line). It also shrinks near the critical regime as N increases. Right Panel: Minimum energy gap as a function of N for a few values of p on semi-log scale. It shows an exponential fall of the minimum gap with N for all values of p according the scaling relation $\Delta_{min} \propto N 2^{-N\alpha}$. Taken from [114].

(b) Application of antiferromagnetic fluctuations

In the context of speed-up of QA, Seki and Nishimori in 2012 proposed a method [115] to overcome issues related to first order phase transitions, by studying quantum annealing in the presence of antiferromagnetic fluctuations in addition to the transverse-field term. They applied the method to the infinite-range ferromagnetic p -spin model (see Eq. (4.1)) and showed that there exists a quantum path that avoids first-order transitions for some intermediate values of p . The Hamiltonian for p -spin is given by

$$H_0 = -N \left(\frac{1}{N} \sum_{i=1}^N \sigma_i^z \right)^p. \quad (4.2)$$

This is indeed the classical counterpart of the Hamiltonian as in Eq. (4.1) with zero transverse field. Here H_0 is the target Hamiltonian H_P , whose ground state is the optimal solution of the problem. The QA for this model is studied before with the transverse-field as a driver Hamiltonian H_D , which takes an exponentially long time to reach the ground state of the target Hamiltonian due to the presence of a quantum first-order phase transition during the time evolution. The ferromagnetic p -spin model reduces to the Grover problem when $p \rightarrow \infty$ and there is no known algorithm that can solve the problem efficiently in a polynomial time.

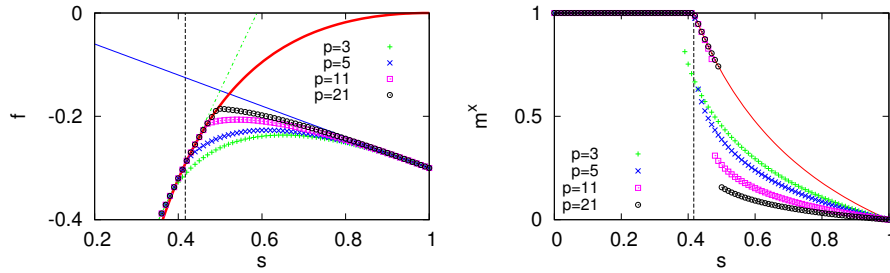


Figure 10. Left panel: Free energy of the system with the Hamiltonian in Eq. (4.3), as a function of s for some values of p with $\lambda = 0.3$. The free energy of the QP phase, Eq. (A.9), is represented by the dash-dotted line in light green. The thin solid line with blue color represents the free energy of the ferromagnetic phase (F), Eq. (A.10), and the thick solid line with red color is for the QP2 phase, Eq. (A.11). The lower limit of the QP2 domain ($s = 1/(3 - 2\lambda)$) is denoted by the vertical dashed line. Although it is hard to see in this present scale, all the data for finite p studied here, have lower values than that of f_{QP2} in the QP2 regime. Right panel: Magnetization m^x vs. s for $\lambda = 0.3$ and the same values of p as in the case of free energies. The vertical dashed line is the same as shown in the left panel. The solid line in red exhibits the x component of magnetization of the QP2 phase. The magnetization decreases to zero as s is increased with a jump at the boundary of the QP2 domain for $p \geq 5$. Taken from [115].

We discuss here how the inclusion of an antiferromagnetic fluctuation term can improve the performance of QA of the model when both the transverse-field term and the antiferromagnetic term are tuned. The total Hamiltonian of the problem is then given by

$$H(s, \lambda) = s\{\lambda H_0 + (1 - \lambda)\hat{V}_{AF}\} + (1 - s)V_{TF}, \quad (4.3)$$

where $V_{AF} = +N\left(\frac{1}{N}\sum_{i=1}^N\sigma_i^x\right)^2$ is an antiferromagnetic interaction term, whereas V_{TF} is the conventional transverse-field term. The parameters s and λ are functions of time, assumed to lie between 0 and 1, which are chosen appropriately for a QA process. The initial Hamiltonian is defined by $s = 0$ and an arbitrary λ , and the final one is given by $s = \lambda = 1$.

(i) Numerical results

We now focus on analyzing the phase diagram of the model on the $s - \lambda$ plane for finite values of p , using the saddle point method and the static approximation, as elaborated in Appendix A. The method we adopt to construct the phase diagram as follows. The self-consistent equations (A.6) and (A.7) are initially solved numerically for a particular value of p and a set of values of s and λ to find out corresponding free energy. By comparing these free energies and all possible solutions, the stable phases of the system are identified with smallest value of free energy. The variation of free energy with s for some values of p and $\lambda = 0.3$ is shown in Fig. 10. It can be seen that the free energies for different values of p lie below f_{QP2} in the QP2 regime and, therefore, the QP2 phase is not a stable phase. As we vary λ , the system undergoes a quantum phase transition from the QP phase for small s to the Ferromagnetic (F) phase for large s .

To determine the type of phase transitions, i.e., first or second order, the magnetization m^x is numerically calculated as a function of s for the same parameter values as in the case of free energy. We observe a change in m^x around $s = 0.4167$ and m^x decreases continuously to zero from its unit value for $p \geq 5$. Equivalently, it indicates that m^z increases continuously from zero to a finite value as we increase s for $p \geq 5$. This identifies that for $p \geq 5$ there exists a second order phase transition at the boundary of QP and QP2 phases. An interesting scenario arises for some parameter values (e.g., $\lambda = 0.3$, $p = 11$) where the magnetization shows a jump within the ferromagnetic phase. This suggests the existence of first-order transition within the F phase and the energy gap at the transition point decreases exponentially with the system size. Nevertheless, this peculiar behavior does not appear for smaller values of λ for any non-zero p , except $p = 3$.

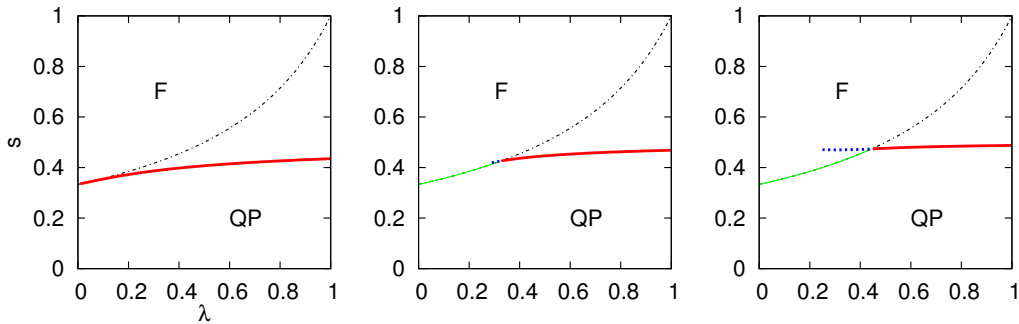


Figure 11. Phase diagrams on the s - λ plane for the system with Hamiltonian in Eq. (4.3) for $p = 3$ (left), $p = 5$ (middle), and $p = 11$ (right). The boundary of the QP2 domain ($s = 1/(3 - 2\lambda)$), where a transition occurs between the QP and F phases, is represented by the dash-dotted line. The red lines are for first-order transitions and the light green lines represent second-order transitions. For $p = 5$ and 11, the magnetization shows sudden jumps on the dashed blue line (F-F boundary) within the F phase. Taken from [115].

Therefore, for smaller λ , there exists only a second order transition when one increase s from zero to a value near unity.

Using these results, phase diagrams of the system for $p = 3, 5$, and 11 are drawn on the $s - \lambda$ plane (see Fig. 11). We can see that a boundary of second-order transitions between F and QP phases exists for small λ and $p \geq 5$. As a consequence, there are possibilities to find a path to reach the F phase from the QP phase by avoiding a first-order transition provided the first-order F-F boundary does not reach the $\lambda = 0$ axis, that occurs probably in the limit of $p \rightarrow \infty$ [115].

Let us now focus on analyzing the behavior of the energy gap across the phase transition points of the system. The energy gap of the system is calculated numerically using perturbation theory as described in Ref. [114]. The variation of energy gap with s for $\lambda = 0.3$ and $p = 11$ is shown in Fig. 12. If the range of s where the energy gap has minimum value is zoomed, it can be seen that the gap shows wiggly behavior throughout the range. This behavior starts at $s \simeq 0.4184$ for $\lambda = 0.3$, which indeed corresponds to the second-order transition point between the QP and F phases. The wiggly behavior ends at $s \simeq 0.4676$ for $\lambda = 0.3$, which corresponds to the first-order transition point at the F-F boundary. The dashed vertical lines in Fig. 12 indicate two transition points that are evaluated analytically using Eqs. A.6 and A.7. The analytical results show nearly a good agreement with the numerical results in the interval where the gap is very small. It has been found that the rightmost local minimum of the energy gap in Fig. 12 corresponding the F-F boundary shows different scaling relation with the system size N compared to the other local minima. The rightmost minimum energy gap decays exponentially with the system size, which is expected from discontinuous behavior of the magnetization in Fig. 10 at the F-F boundary implying the first-order transition. Although, for the present case, the above mentioned energy gap is not a global minimum, this will affect the efficiency of QA for larger systems where the rightmost gap can become a global minimum since the other local minima decay polynomially with the system sizes (see Figs. 6 and 7 of [115] for details).

These analytical and numerical results suggest that it is possible to increase the efficiency of QA by choosing a path around $\lambda = 0.1$, which avoids first-order transition to reach the F phase from the QP phase. For this process, s is the tuning parameter and the value p needs to be chosen within the range $5 \leq p \leq 21$ achieving maximum efficiency.

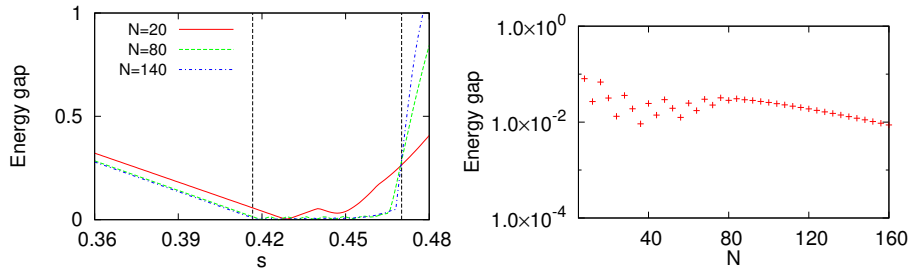


Figure 12. Left panel: Energy gap as a function of s for $p = 11$ and $\lambda = 0.3$. The positions of minima of the energy gap are shown by the vertical dashed lines at the QP2 domain with $s \simeq 0.4167$ and the F-F boundary at $s \simeq 0.4701$. Right panel: The rightmost local minimum of the energy gap with the system size N for $p = 11$ and $\lambda = 0.3$ on a semi-log scale. The energy gap closes exponentially fast with N . Taken from [115].

(c) Inhomogenous transverse field driving

In Sec. 4(b), we have discussed a method to speed up a QA process in the presence of first order phase transitions by adding an antiferromagnetic fluctuation term. Here we consider a relatively simpler approach of inhomogenous driving of the transverse field to overcome the issue of first order phase transitions. In this case, the strength of transverse field is turned off sequentially from one site to the next according to the annealing schedule. Using both analytical and numerical calculations, it has been shown that inhomogenous driving can completely remove QPTs from the annealing path and thus, it speeds up the annealing process exponentially [116,117].

The total Hamiltonian for the inhomogenous driving is given by

$$H(s, \tau) = sH_0 - \sum_{i=1}^{N(1-\tau)} \sigma_i^x, \quad (4.4)$$

where H_0 is the Hamiltonian for p -spin model in Eq. (4.2). The parameters s and τ both are time-dependent, where $s = \tau = 0$ at $t = 0$ and $s = \tau = 1$ at $t = t_0$. This shows that the initial Hamiltonian has only transverse field and the final one has only p -spin interacting term with the Hamiltonian H_0 . Both the initial and final Hamiltonians are in agreement with the traditional QA protocol.

We note that the transverse field in Eq. (4.4) is applied only to $N(1 - \tau)$ spins, where τ increases from 0 to 1 as time proceeds from 0 to t_0 . This indicates that the transverse field is turned off at neighbouring sites one by one as time increases, starting from site $i = N$ to ending with site $i = 1$ at $\tau = 1$. This is the process of how the transverse field is driven inhomogeneously. It can be noted that the parameter τ can have only discrete values for a finite N , since the upper limit $N(1 - \tau)$ in Eq. (4.4) should be an integer.

(i) Results

Using Trotter decomposition and the static approximation in Hamiltonian (4.4), the free energy of the system can be calculated analytically for both finite and zero temperatures (see appendix B). By minimizing the zero-temperature free energy with respect to magnetization m produces a ground state phase diagram as depicted in Fig. 13.

For a fixed value of p , a line of first-order phase transitions originated from a point on the s -axis, terminates before approaching to any point of the τ -axis. Remarkably, all these lines for different values of p end before they reach one of the axes, $\tau = 1$ or $s = 0$. Therefore, there exists a path starting from $s = \tau = 0$ to $s = \tau = 1$, that does not encounter any kind of phase transitions. This leads to an exponential speedup of QA, since the energy gap always remains finite even

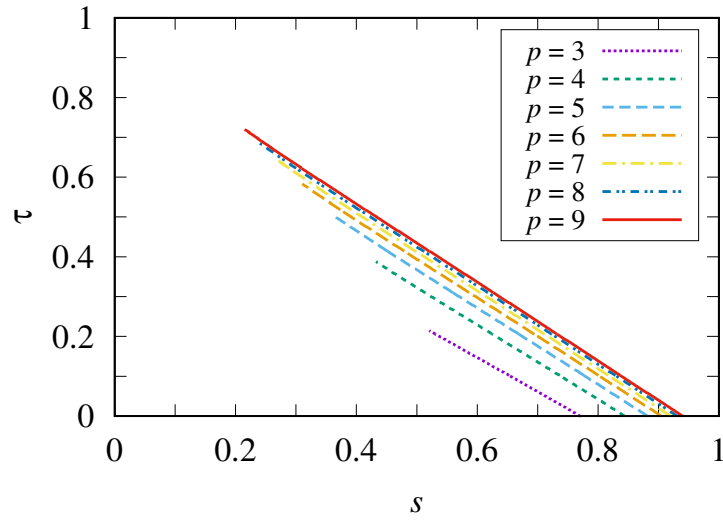


Figure 13. Phase diagram of the p -spin ferromagnetic model under inhomogeneous field. All the lines represent first-order phase transitions for different values of p , which are extended up to the middle of the phase diagram from the axis $\tau = 0$ corresponding to the homogeneous model. Taken from [116].

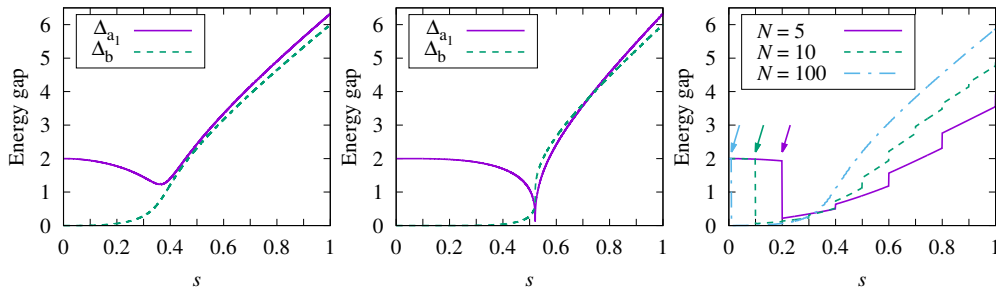


Figure 14. Plots of two types of energy gap Δ_{a_1} and Δ_b for $p = 3$ as functions of s with (left) $\tau = s$ (i.e., away from the transition line) and (middle) $\tau = s^{2.366}$ (i.e., just touches the critical point). The final energy gap is defined by the smaller of these two gaps. Right: The energy gap for different system sizes with $\tau = s$ computed by direct numerical diagonalization. The location of the minimum energy gap is shown by an arrow for each N . Taken from [117].

for a system with large size. The positions of the critical points on the $\tau - s$ plane where the first-order transitions terminate for different p values, are calculated analytically by using the standard Landau theory of phase transitions (see Eq. (B.3)). In this calculation, it has been considered that the coefficients of the expansion of the free energy (B.2) around its minimum at $m = m_c$ vanish to third order [118].

To strengthen the above conclusion, the energy gap of the system has been calculated both analytically and numerically. Since our system is mean-field-type, the semi-classical treatment can be applied to evaluate the energy gap [119,120]. In this context, the parameterization of a path $\tau = s^r$ is considered to connect $s = \tau = 0$ and $s = \tau = 1$ with a parameter r that determines the shape of the path. Figures i and i exhibit two energy gap candidates, Δ_{a_1} and Δ_b , for the system with $p = 3$ along the paths $\tau = s$, that does not encounter phase transitions, and $\tau = s^{2.366}$, that just touches the critical point where the first-order line ends. The smaller one between these two candidates is the actual energy gap of the system.

As shown in Fig. i, Δ_b is found to be smaller one and, it monotonically increases with s . On the other hand, as expected, the energy gap Δ_{a_1} vanishes at the critical point $s_c \approx 0.52$. To investigate the effect of finite-size systems, the energy gap is calculated by a direct numerical diagonalization method along the $\tau = s$ path. The result is shown in Fig. i, which shows a very good agreement with the asymptotic behavior in the $N \rightarrow \infty$ limit as observed in Δ_b of Fig. i. As seen in Fig. (i), the energy gap becomes minimum when the transverse field is turned off at the first site as shown by the arrows, thus implying the location of the minimum gap at $s = 0$ in the $N \rightarrow \infty$ limit. It is important to note that the the energy gap becomes minimum near the origin $\tau = s = 0$, when the annealing path ($\tau = s$) does not encounter any transitions (see Figs. i and i), whereas the minimum of the gap occurs at the critical point when such a transition exists along the path (see Fig. i). In addition, a series of paths is considered to examine the inhomogenous driving protocol, and it is found that the minimum energy gap shows an exponential decrement with the system sizes when the paths cross the first order transitions (for details, refer to the discussion around Eq. (12) of Ref. [117]).

The problem that we discussed so far, for inhomogeneous driving, considers ideal situations, i.e., zero temperature and a complete turning off of the transverse field at each site. This problem also has been studied at finite temperature and zero temperature with different types of inhomogeneity. It has already been studied that the first-order transitions that exists under homogeneous driving at zero temperature can be circumvented by inhomogeneous driving with complete turning off the transverse field at each site. For nonideal situations, with a finite temperature or a non-zero value of the final transverse field, one can not avoid new first-order transition lines like the ideal case. Nevertheless, it has been observed that the new first-order transitions are weaker than the original one, since the free energy barrier between two arbitrary local minima is smaller than the original homogeneous case. This leads to an increase in the quantum tunneling rate. Therefore one can infer that the inhomogeneous driving of the transverse field has the potential to provide a better performance in quantum annealing. In addition, Matsuura et al. [121] studied analytically the p -body ferromagnetic infinite-range Ising model in transverse-field using a mean-field analysis and demonstrated that for $p \geq 3$, where the phase transition is of first order, Quantum Annealing Correction softens the closing of the gap for small energy penalty values and prevents its closure for sufficiently large energy penalty values, thereby providing from excitations that occur near the quantum critical point. It also has been shown analytically that nested quantum annealing correction can suppress errors effectively in Ising models with infinite-range interactions and their analysis revealed that the nesting structure can significantly weaken or remove the first-order phase transitions, where the energy gap closes exponentially [122].

(d) Suppression of Griffiths singularities

In a recent work by Knysh et al. [123], it has been shown that a QA process can be accelerated using an embedded spin chain system with random interactions. A randomly interacting spin chain exhibits Griffiths-McCoy singularities [124,125], since different parts of the system can not reach criticality simultaneously for random fluctuations. This leads to the diverging dynamical exponent z and a stretched exponential scaling of the energy gap [36]. Therefore the presence of Griffiths singularities increases the annealing time for such systems.

On the other hand, quantum annealing has been studied for a embedded spin chain problem, where logical qubits were replaced by ferromagnetic Ising spin chains [123]. For this study, an ansatz is considered to find a balanced choice of coupling parameters based on renormalization group intuition for the better performance of QA. This results an exponential improvement of annealing time, which is also confirmed numerically. It indicates that this protocol prevents to occur randomly oriented domains in the system by ensuring a simultaneous criticality of spatially separated regions.

5. Application

In this section, we discuss some recent results on QA of a interacting bosonic system coupled with cavity field modes for both classical and quantum limits of the system. In addition, we will mention about the recent development of QA in context of parallel computation, and its effectiveness compared to the existing methods.

(a) Quantum annealing vs. semi-classical annealing

Starchl and Ritsch [17], have used the idea of quantum tunneling to show the success of QA over semi-classical annealing for an interacting bosonic model in presence of cavity modes. The model that is considered for this study is described by a tight binding Bose-Hubbard lattice model with four sites, which are filled by two interacting bosons. The tunable non-local interactions are introduced in the model via collective light scattering to two independent cavity modes. The Hamiltonian for such system is given by

$$\begin{aligned}
 H &= J \sum_{kPBC} (b_k^\dagger b_{k+1} + h.c.) + \frac{U}{2} \sum_k n_k (n_k - 1) \\
 &- \Delta (a_1^\dagger a_1 + a_2^\dagger a_2) + \tilde{J} (\hat{M}_1 (a_1 + a_1^\dagger) + \hat{M}_2 (a_2 + a_2^\dagger)),
 \end{aligned} \tag{5.1}$$

where b_k and b_k^\dagger are bosonic annihilation and creation operators, respectively. The photonic annihilation operators a_1 and a_2 are associated with two independent cavity modes. The interactions between the bosons and cavity field modes are represented by the fourth term of Eq. (5.1), where \hat{M}_1 and \hat{M}_2 are called effective scattering operators. Using mean-field approximation of the field operators, the Hamiltonian in Eq. (5.1) can be written in semiclassical form

$$H^{sc} = \frac{\Delta \tilde{J}^2}{\kappa^2 + \Delta^2} (2\hat{M}_1 \langle \hat{M}_1 \rangle - \hat{I} \langle \hat{M}_1 \rangle^2 + 2\hat{M}_2 \langle \hat{M}_2 \rangle - \hat{I} \langle \hat{M}_2 \rangle^2), \tag{5.2}$$

where κ determines the strength of cavity loss, where I denotes the identity operator. Both the Hamiltonians in Eqs. (5.1) and (5.2) with periodic boundary conditions are translationally invariant and thus provide approximately degenerate ground states. In order to create a unique target ground state for the annealing process, a certain amount of impurity of strength V is added in the Hamiltonian.

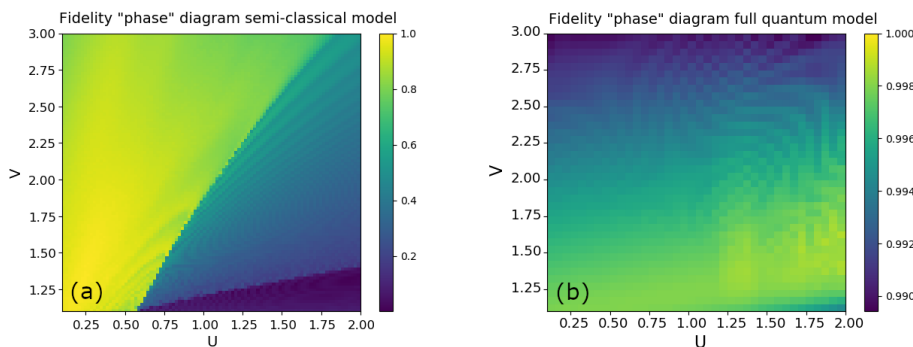


Figure 15. Color density plot of the fidelity calculated as the overlap between the final state after an adiabatic evolution using (a) the Hamiltonian with semi-classical mean-field approximation and as well as (b) for the full quantum Hamiltonian, and the desired target state on the $U - V$ plane. Here the parameter values are: $t_f = 1000$. For (a): $\Delta = -1$, $\tilde{J} = 1$ and for (b): $\Delta = -5$, $\tilde{J} = \sqrt{5}$. Taken from [17].

The dynamics of the system is started with the ground state at zero pump $\tilde{J} = 0$, and the pump strength is increased linearly towards $\tilde{J} = \sqrt{5}$, following an adiabatic schedule: $\tilde{J} \approx t/t_f$, where t_f is the final time. The results of the study of annealing for this system are summarized in Fig. 15. It shows the density plot of the fidelity on $U - V$ plane after an adiabatic sweep using both the semi-classical (5.1) and the full quantum (5.2) Hamiltonian. In this case, the fidelity is calculated as the overlap between the final state after an adiabatic sweep and the desired target state. By comparing two density plots for both semi-classical and quantum cases, i.e., when the dynamics is driven by the semi-classical Hamiltonian and the full quantum Hamiltonian, respectively, one can identify a clear quantum improvement in the success rate. It is observed that the semi-classical approximation provides a reliably correct solution for small onsite interaction strength. For this scenario, one can see a sudden fall of the success rate, when the interaction strength is increased. If the repulsive interaction is further increased, the gap between the final ground state energy and the first excitation becomes very small and the classical model effectively never succeeds. On the other hand, the adiabatic evolution with full quantum Hamiltonian (5.1) provides almost correct solution with 99% probability, even for higher U values as shown in Fig. 15(b). Therefore, for this system, a large parameter region is found where quantum annealing is highly successful, whereas the semi-classical approach largely fails. In addition, for quantum scenario, a direct connection is found between atom-field entanglement in the dynamics and a high probability to find the correct solution at end of annealing process.

(b) Parallel quantum annealing

There are a few recent studies on QA in the context of parallel quantum computation [126–128]. Recently, Pelofske et al. [128] propose a method named as parallel quantum annealing that has potential to solve many independent problems on a quantum annealer during the same annealing process. The authors applied their proposed method of parallel quantum annealing on both D-Wave 2000Q at Los Alamos National Laboratory (refereed to as D-W 2000Q) and the newer D-Wave Advantage_System 1.1 (referred to as D-W Advantage). The results of parallel quantum annealing have been compared with those found from sequential quantum annealing, i.e., when the same problems are solved sequentially on D-Wave machine. It has been observed that, although, there is a slight decrement in the accuracy of the solution for simultaneously solved problems, parallel quantum annealing can provide a considerable speedup of up to two orders of magnitude [128].

6. Summary and outlook

We have provided an overview of recent developments of QA which is based on the possible advantage of utilizing quantum tunneling. When the energy landscape of an Ising Hamiltonian, where the corresponding ground state is the target state of an optimisation problem, consists of high but thin barriers surrounding local minima, quantum tunneling has an advantage over thermal fluctuation in overcoming barriers and thus getting the system equilibrated. This nature of quantum tunneling provides a foundation which asserts that QA can outperform SA in a glassy system with a rugged energy landscape. Indeed, we have focused on analytical and numerical evidences that QA yields a better solution than SA in several glassy systems. The question of the restoration of ergodicity due to quantum tunneling in the quantum SK model is still unresolved. Nevertheless, recent studies do indicate the possibility of the existence of an ergodic phase at least in low temperature region [62,64]: this is expected to lead to a remarkable possibility of the success of the annealing scheme in those systems [61].

We have also discussed quantum phase transitions (QPTs) in connection with QA. Generally speaking, a QPT hinders the adiabatic time evolution underlying QA, since the energy gap above the ground state closes at a QPT; this leads to inevitable generation of defects and excess energy in the final evolved state. In this context, it is worth noting that the short-cut to adiabaticity [129] or counter-diabatic driving protocols [130] have been proposed as a method to realize the adiabatic

time evolution with a finite time, providing a possible route to avoid a continuous QPT in the process of annealing. On the contrary, a discontinuous QPT involves an exponentially fast closure of the energy gap with the system size. Therefore, it is desirable and at the same time far more challenging to circumvent a discontinuous QPT for the success of QA. We have reviewed methods using additional antiferromagnetic interactions [123] or inhomogeneous transverse fields [116,117] proposed for avoiding discontinuous QPTs which would lead to acceleration of QA. Random interactions in spin chain systems induce Griffiths singularities that eventually increase annealing time for such systems. These singularities can be suppressed for the embedded spin chain problem, where ferromagnetic Ising spin chains are used as logical qubits. It has been shown that the performance of QA for such embedded systems improves exponentially in the context of annealing time [123]. To be precise, the performance advantage of QA is still model specific and a generic prescription has not been known for discontinuous phase transitions involved by practical optimization problems. In the cases of spin glass models, however, major advantages of the standard QA have now even been established using QMC simulation [79] and hardware implementations [85,131,132].

The idea of quantum tunneling has been further used by Starchl and Ritsch [17] to establish the superiority of QA over semi-classical annealing for a realistic system of interacting bosons in presence of cavity modes. Using numerical results, it has been shown that there exists a large parameter regime where the QA provides a better performance than semi-classical annealing. In addition, we have noted the recent development of parallel quantum computation using an annealing algorithm [128]. The idea of parallel QA is to solve many independent problems on a quantum annealer during the same annealing schedule. The authors have checked their method of parallel QA on D-wave quantum machines and indicated the effectiveness of the same [128].

Finally, in recent years the progress in developing hardware that performs QA using physical qubits has gained a tremendous momentum. So far, devices with more than 5000 qubits have been made available, and employed to study a wide gamut of fields that include condensed matter systems in and out of equilibrium [93,131,133–135], high-energy physics [136–138], quantum chemistry [139], and biology [140,141]. Application to various optimization problems has been developing as well. We reviewed some of the experimental studies using a QA hardware. From the viewpoint of application as well as gaining theoretical rigor, decoherence inherent in a device coupled to an environment is a fundamental issue of interest. We have briefly reviewed effects of thermal and non-thermal environments on QA. In order to perform QA ideally, coupling to an environment leading to decoherence should be reduced. However, environment assisted QAs have been proposed for specific situations [142–144]. Utilising specially engineered environments to accelerate QA would be an important direction of future study.

A. Static approximation and low-temperature limit

Using Suzuki-Trotter formula, the partition function for the Hamiltonian in Eq. (4.3) can be written as

$$\begin{aligned}
 Z &= \lim_{M \rightarrow \infty} Z_M \\
 &= \lim_{M \rightarrow \infty} \text{Tr} \left(e^{-\frac{\beta}{M} s \lambda H_0} e^{-\frac{\beta}{M} \{s(1-\lambda)V_{\text{AFF}} + (1-s)V_{\text{TF}}\}} \right)^M \\
 &= \lim_{M \rightarrow \infty} \sum_{\{\sigma_i^z\}} \langle \{\sigma_i^z\} | \left(\exp \left[\frac{\beta s \lambda N}{M} \left(\frac{1}{N} \sum_{i=1}^N \sigma_i^z \right)^p \right] \right. \\
 &\quad \left. \times \exp \left[-\frac{\beta s(1-\lambda)N}{M} \left(\frac{1}{N} \sum_{i=1}^N \sigma_i^x \right)^2 + \frac{\beta(1-s)}{M} \sum_{i=1}^N \sigma_i^x \right] \right)^M | \{\sigma_i^z\} \rangle, \quad (\text{A.1})
 \end{aligned}$$

where $\sum_{\{\sigma_i^z\}}$ denotes the summation over all spin configurations in the z basis, and $|\{\sigma_i^z\}\rangle \equiv \bigotimes_{i=1}^N |\sigma_i^z\rangle$. The state $|\sigma_i^z\rangle$ is the eigenstate of σ_i^z , having the eigenvalue σ_i^z ($=\pm 1$). Similar notations will be used for the x basis.

Following saddle point method in the limit $N \rightarrow \infty$ and static approximation (i.e., neglecting the imaginary-time dependence of the partition function in Eq. (A.1) [114,115,145]), the partition function of the system can be written as

$$Z = \iint dm^z dm^x \exp[-N\beta f(\beta, s, \lambda; m^z, m^x)], \quad (\text{A.2})$$

where $f(\beta, s, \lambda; m^z, m^x)$ is the pseudo free energy defined as follows:

$$f(\beta, s, \lambda; m^z, m^x) = (p-1)s\lambda(m^z)^p - s(1-\lambda)(m^x)^2 - \frac{1}{\beta} \ln 2 \cosh \beta \sqrt{\{ps\lambda(m^z)^{p-1}\}^2 + \{1-s-2s(1-\lambda)m^x\}^2}. \quad (\text{A.3})$$

The saddle point equations are thus

$$m^z = \frac{ps\lambda(m^z)^{p-1}}{\sqrt{\{ps\lambda(m^z)^{p-1}\}^2 + \{1-s-2s(1-\lambda)m^x\}^2}} \times \tanh \beta \sqrt{\{ps\lambda(m^z)^{p-1}\}^2 + \{1-s-2s(1-\lambda)m^x\}^2}, \quad (\text{A.4})$$

$$m^x = \frac{1-s-2s(1-\lambda)m^x}{\sqrt{\{ps\lambda(m^z)^{p-1}\}^2 + \{1-s-2s(1-\lambda)m^x\}^2}} \times \tanh \beta \sqrt{\{ps\lambda(m^z)^{p-1}\}^2 + \{1-s-2s(1-\lambda)m^x\}^2}. \quad (\text{A.5})$$

To examine quantum phase transitions of the model, we consider low-temperature limits of the above self-consistent equations. For a finite value of the square root in Eq. (A.4) and Eq. (A.5), the hyperbolic tangent tends to unity in the limit of $\beta \rightarrow \infty$. Then the equations are given as

$$m^z = \frac{ps\lambda(m^z)^{p-1}}{\sqrt{\{ps\lambda(m^z)^{p-1}\}^2 + \{1-s-2s(1-\lambda)m^x\}^2}}, \quad (\text{A.6})$$

$$m^x = \frac{1-s-2s(1-\lambda)m^x}{\sqrt{\{ps\lambda(m^z)^{p-1}\}^2 + \{1-s-2s(1-\lambda)m^x\}^2}}. \quad (\text{A.7})$$

In that case, the pseudo free energy (A.3) becomes

$$f(s, \lambda; m^z, m^x) = (p-1)s\lambda(m^z)^p - s(1-\lambda)(m^x)^2 - \sqrt{\{ps\lambda(m^z)^{p-1}\}^2 + \{1-s-2s(1-\lambda)m^x\}^2}. \quad (\text{A.8})$$

Equations (A.6) and (A.7) provide a ferromagnetic (F) solution with $m^z > 0$ and a quantum paramagnetic (QP) solution for $m^z = 0$ and $m^x \neq 0$. Using these properties of a quantum paramagnetic phase, the regions of QP phases can be found on the $s - \lambda$ plane. It appears that there exists two types of QP phases in this problem and we call them QP and QP2 phases to distinguish from each other.

The regions of the different phases in terms of system parameters can be calculated using the above conditions of those phases in Eqs. (A.6) and (A.7). It has been found that the QP phase exists in the region $0 \leq s < 1/(3-2\lambda)$, and its free energy is given by

$$f_{\text{QP}}(s, \lambda) = -s\lambda + 2s - 1, \quad (\text{A.9})$$

which is independent of p . The free energy of the F phase can not be calculated analytically for a general p from Eqs. (A.6) and (A.7). However, in the limit of $p \rightarrow \infty$, the free energy of the F phase

is given as

$$f_{\text{F}}(s, \lambda)|_{p \rightarrow \infty} = -s\lambda. \quad (\text{A.10})$$

The free energy of the QP2 phase is given by

$$f_{\text{QP2}}(s, \lambda) = -\frac{(1-s)^2}{4s(1-\lambda)}, \quad (\text{A.11})$$

with the domain of applicability is restricted by $1/(3-2\lambda) \leq s < 1$.

B. Inhomogenous driving of the transverse field

(a) Free energy and first-order transitions

By applying Trotter decomposition and the static approximation on the Hamiltonian in Eq. (4.4), the resulting free energy at finite temperature is given by [116]

$$\begin{aligned} f(m; s, \tau) &= (1-\tau) \left\{ (p-1)sm^p - T \log 2 \cosh \beta \sqrt{(spm^{p-1})^2 + 1} \right\} \\ &\quad + \tau \left\{ (p-1)sm^p - T \log 2 \cosh(\beta spm^{p-1}) \right\}, \end{aligned} \quad (\text{B.1})$$

where m is the magnetization of the system along the z axis. In the limit of zero temperature, the free energy takes form

$$\begin{aligned} f_0(m; s, \tau) &= (1-\tau) \left\{ (p-1)sm^p - \sqrt{(spm^{p-1})^2 + 1} \right\} \\ &\quad + \tau \left\{ (p-1)sm^p - spm^{p-1} \right\}. \end{aligned} \quad (\text{B.2})$$

For the calculation of zero-temperature free energy it has been assumed that $m \geq 0$.

Using the standard Landau theory of phase transitions, the locations of the critical points s_c , τ_c (see Fig. 13) where the first-order transition lines terminate for different p , can be found as

$$\tau_c = \frac{1}{1 + \sqrt{\frac{27(p-1)}{4(p-2)^3}}}, \quad s_c = \frac{1}{pm_c^{p-1} \sqrt{1 - m_{1c}^2/m_{1c}}}, \quad (\text{B.3})$$

where $m_{1c} = \sqrt{(p-2)/(3(p-1))}$ and $m_c = \tau_c + (1-\tau_c)m_{1c}$.

(b) Semiclassical theory of energy gap

One can rewrite the Hamiltonian (4.4) in terms of two macroscopic spin operators (for details see Refs. [116,117]),

$$S_1^{z,x} = \frac{1}{2} \sum_{i=1}^{N(1-s^r)} \sigma_i^{z,x}, \quad S_2^{z,x} = \frac{1}{2} \sum_{i=N(1-s^r)+1}^N \sigma_i^{z,x} \quad (\text{B.4})$$

as

$$H(s, \tau) = -sN \left\{ \frac{2}{N} (S_1^z + S_2^z) \right\}^p - 2S_1^x. \quad (\text{B.5})$$

These giant operators can be considered as classical vectors for sufficiently large N , and the quantum fluctuations are subsequently applied around the classically stable directions through an expansion of the Holstein-Primakoff transformation to the quadratic order in terms of boson

operators, as done in Refs. [119,120]. The result is given as

$$H(s, \tau) = Ne + \gamma + \frac{\delta}{2}(\sqrt{1 - \epsilon^2} - 1) + \Delta_{a_1} \tilde{a}_1^\dagger \tilde{a}_1 + \Delta_{a_2} \tilde{a}_2^\dagger \tilde{a}_2 + \Delta_b b^\dagger b, \quad (\text{B.6})$$

where \tilde{a}_1 and \tilde{a}_2 are bosonic annihilation operators, and e is the energy per spin of the classical ground-state. The parameters Δ_{a_1} , Δ_{a_2} and Δ_b represent quantum fluctuations, where

$$\Delta_{a_1} = \delta \sqrt{1 - \epsilon^2}, \quad \Delta_{a_2} = \delta. \quad (\text{B.7})$$

Because $\Delta_{a_2} \geq \Delta_{a_1}$, the minimum energy gap of the system is the smaller of Δ_{a_1} and Δ_b :

$$\Delta = \min(\Delta_{a_1}, \Delta_b) \\ \Delta_{a_1} = \delta \sqrt{1 - \epsilon^2}, \quad \Delta_b = 2sp\{\tau + (1 - \tau) \cos \theta_0\}^{p-1}, \quad (\text{B.8})$$

where

$$\theta_0 = \arg \min_{\theta} \{-s[\tau + (1 - \tau) \cos \theta]^p - (1 - \tau) \sin \theta\} \\ \epsilon = -\frac{2\gamma}{\delta}, \\ \gamma = -\frac{1}{2}sp(p-1)(1-\tau) \sin^2 \theta_0 \{\tau + (1 - \tau) \cos \theta_0\}^{p-2}, \\ \delta = \Delta_b \cos \theta_0 + 2 \sin \theta_0 + 2\gamma. \quad (\text{B.9})$$

Ethics. NA.

Data Accessibility. The article has no additional data over those given in different figures taken from published papers.

Authors' Contributions. AD and BKC conceptualized the review. AR and SS contributed to materials and organised it. All authors contributed to editing and finalizing the review.

Competing Interests. We declare, we do not have any competing interests.

Funding. A.R. acknowledges UGC, India for Start-up Research Grant No. F. 30-509/2020(BSR). The work of S.S. was supported by JSPS KAKENHI Grant No. 22K03455. A.D. acknowledges support from SPARC program, MHRD, India and SERB, DST, New Delhi, India. BKC is grateful to the Indian National Science Academy for their Senior Scientist Research Grant.

Acknowledgements. We acknowledge our collaborations with Gabriel Aeppli, Arunava Chakrabarti, Arnab Das, Uma Divakaran, Jun-ichi Inoue, Sudip Mukherjee, Hidetoshi Nishimori, Masato Okada, Purusattam Ray, Thomas F. Rosenbaum, Diptiman Sen, Parongama Sen, Robin B. Stinchcombe, Ryo Tamura and Shu Tanaka on this development. AD acknowledges Souvik Bandyopadhyay and Sourav Bhattacharjee for comments. We are grateful to the anonymous referees for their useful comments and important suggestions.

Disclaimer. This review is limited by our personal knowledge and also by the size limit (which we have already crossed). We do not claim any completeness of discussions on even some important contributions in this incredibly active field of research.

References

1. A. B. Finnila, M. A. Gomez, C. Sebenik, et al.
Quantum annealing: A new method for minimizing multidimensional functions.
Chem. Phys. Lett., 219, 343 (1994).
2. T. Kadowaki and H. Nishimori.
Quantum annealing in the transverse Ising model.

- Phys. Rev. E*, 58, 5355 (1998).
3. E. Farhi, J. Goldstone, S. Gutmann, et al.
A Quantum Adiabatic Evolution Algorithm Applied to Random Instances of an NP-Complete Problem.
Science, 292, 472 (2001).
 4. G. E. Santoro and E. Tosatti.
Optimization using quantum mechanics: quantum annealing through adiabatic evolution.
J. Phys. A: Math. Gen., 39, R393 (2006).
 5. A. Das and B. K. Chakrabarti.
Colloquium: Quantum annealing and analog quantum computation.
Rev. Mod. Phys., 80, 1061 (2008).
 6. S. Morita and H. Nishimori.
Mathematical foundation of quantum annealing.
J. Math. Phys., 49, 125210 (2008).
 7. S. Tanaka, R. Tamura, and B. K. Chakrabarti.
Quantum spin glasses, annealing and computation.
Cambridge University Press (2017).
 8. T. Albash and D. A. Lidar.
Adiabatic quantum computation.
Rev. Mod. Phys., 90, 015002 (2018).
 9. P. Hauke, H. G. Katzgraber, W. Lechner, et al.
Perspectives of quantum annealing: Methods and implementations.
Rep. Prog. Phys., 83, 054401 (2020).
 10. A. Das, B. K. Chakrabarti, and R. B. Stinchcombe.
Quantum annealing in a kinetically constrained system.
Phys. Rev. E, 72, 026701 (2005).
 11. A. Messiah.
Quantum Mechanics.
North Holland, Amsterdam (1961).
 12. S. Suzuki and M. Okada.
Residual energies after slow quantum annealing.
J. Phys. Soc. Jpn., 74, 1649 (2005).
 13. S. Kirkpatrick, C. D. Gelatt Jr, and M. P. Vecchi.
Optimization by simulated annealing.
science, 220, 671 (1983).
 14. R. Shankar.
Principles of quantum mechanics.
Springer (2012).
 15. S. Mukherjee and B. K. Chakrabarti.
Multivariable optimization: Quantum annealing and computation.
Eur. Phys. J. ST, 224, 17 (2015).
 16. P. Ray, B. K. Chakrabarti, and A. Chakrabarti.
Sherrington-Kirkpatrick model in a transverse field: Absence of replica symmetry breaking due to quantum fluctuations.
Phys. Rev. B, 39, 11828 (1989).
 17. E. A. Starchl and H. Ritsch.
Unraveling the origin of higher success probabilities in quantum annealing versus semi-classical annealing.
J. Phys. B: Atomic, Molecular and Optical Physics (2022).
 18. D. Sherrington and S. Kirkpatrick.
Solvable model of a spin-glass.
Phys. Rev. Lett., 35, 1792 (1975).
 19. R. Yaacoby, N. Schaar, L. Kellerhals, et al.
Comparison between a quantum annealer and a classical approximation algorithm for computing the ground state of an Ising spin glass.
Phys. Rev. E, 105, 035305 (2022).
 20. S. L. Sondhi, S. Girvin, J. Carini, et al.
Continuous quantum phase transitions.
Rev. Mod. Phys., 69, 315 (1997).

21. S. Sachdev.
Quantum Phase Transitions.
Cambridge University Press, Cambridge (1999).
22. S. Suzuki, J.-i. Inoue, and B. K. Chakrabarti.
Quantum Ising phases and transitions in transverse Ising models, volume 862.
Springer (2012).
23. A. Dutta, G. Aeppli, B. K. Chakrabarti, et al.
Quantum phase transitions in transverse field spin models: from statistical physics to quantum information.
Cambridge University Press (2015).
24. T. W. B. Kibble.
Topology of cosmic domains and strings.
J. Phys. A: Math. Gen., 9, 1387 (1976).
25. W. H. Zurek.
Cosmological experiments in superfluid helium?
Nature, 317, 505 (1985).
26. W. H. Zurek, U. Dorner, and P. Zoller.
Dynamics of a Quantum Phase Transition.
Phys. Rev. Lett., 95, 105701 (2005).
27. A. Polkovnikov.
Universal adiabatic dynamics in the vicinity of a quantum critical point.
Phys. Rev. B, 72, 161201 (2005).
28. B. Damski.
The simplest quantum model supporting the Kibble-Zurek mechanism of topological defect production: Landau-Zener transitions from a new perspective.
Phys. Rev. Lett., 95, 035701 (2005).
29. V. Mukherjee, U. Divakaran, A. Dutta, et al.
Quenching dynamics of a quantum X Y spin-1 2 chain in a transverse field.
Phys. Rev. B, 76, 174303 (2007).
30. D. Sen, K. Sengupta, and S. Mondal.
Defect production in nonlinear quench across a quantum critical point.
Phys. Rev. Lett., 101, 016806 (2008).
31. R. Barankov and A. Polkovnikov.
Optimal nonlinear passage through a quantum critical point.
Phys. Rev. Lett., 101, 076801 (2008).
32. V. Mukherjee and A. Dutta.
Adiabatic multicritical quantum quenches: Continuously varying exponents depending on the direction of quenching.
EPL (Europhysics Lett.), 92, 37004 (2010).
33. J. Dziarmaga.
Dynamics of a quantum phase transition and relaxation to a steady state.
Adv. Phys., 59, 1063 (2010).
34. A. Polkovnikov, K. Sengupta, A. Silva, et al.
Colloquium: Nonequilibrium dynamics of closed interacting quantum systems.
Rev. Mod. Phys., 83, 863 (2011).
35. J. Dziarmaga.
Dynamics of a Quantum Phase Transition: Exact Solution of the Quantum Ising Model.
Phys. Rev. Lett., 95, 245701 (2005).
36. D. S. Fisher.
Random transverse field Ising spin chains.
Phys. Rev. Lett., 69, 534 (1992).
37. D. S. Fisher.
Critical behavior of random transverse-field Ising spin chains.
Phys. Rev. B, 51, 6411 (1995).
38. A. P. Young and H. Rieger.
Numerical study of the random transverse-field Ising spin chain.
Phys. Rev. B, 53, 8486 (1996).
39. D. S. Fisher and A. P. Young.

- Distributions of gaps and end-to-end correlations in random transverse-field Ising spin chains.
Phys. Rev. B, 58, 9131 (1998).
40. J. Dziarmaga.
Dynamics of a quantum phase transition in the random Ising model: Logarithmic dependence of the defect density on the transition rate.
Phys. Rev. B, 74, 064416 (2006).
41. T. Caneva, R. Fazio, and G. E. Santoro.
Adiabatic quantum dynamics of a random Ising chain across its quantum critical point.
Phys. Rev. B, 76, 144427 (2007).
42. S. Suzuki.
Cooling dynamics of pure and random Ising chains.
J. Stat. Mech. Theory Exp., 2009, P03032 (2009).
43. M. Schmitt, M. M. Rams, J. Dziarmaga, et al.
Quantum phase transition dynamics in the two-dimensional transverse-field Ising model (2021).
44. R. Botet and R. Jullien.
Large-size critical behavior of infinitely coordinated systems.
Phys. Rev. B, 28, 3955 (1983).
45. O. L. Acevedo, L. Quiroga, F. J. Rodríguez, et al.
New Dynamical Scaling Universality for Quantum Networks Across Adiabatic Quantum Phase Transitions.
Phys. Rev. Lett., 112, 030403 (2014).
46. S. F. Edwards and P. W. Anderson.
Theory of spin glasses.
J. Phys. F: Metal Phys., 5, 965 (1975).
47. B. K. Chakrabarti.
Critical behavior of the Ising spin-glass models in a transverse field.
Phys. Rev. B, 24, 4062 (1981).
48. H. Rieger and A. P. Young.
Zero-temperature quantum phase transition of a two-dimensional Ising spin glass.
Phys. Rev. Lett., 72, 4141 (1994).
49. M. Guo, R. N. Bhatt, and D. A. Huse.
Quantum critical behavior of a three-dimensional Ising spin glass in a transverse magnetic field.
Phys. Rev. Lett., 72, 4137 (1994).
50. R. R. P. Singh and A. P. Young.
Critical and Griffiths-McCoy singularities in quantum Ising spin glasses on d -dimensional hypercubic lattices: A series expansion study.
Phys. Rev. E, 96, 022139 (2017).
51. R. Miyazaki and H. Nishimori.
Real-space renormalization-group approach to the random transverse-field Ising model in finite dimensions.
Phys. Rev. E, 87, 032154 (2013).
52. D. A. Matoz-Fernandez and F. Romá.
Unconventional critical activated scaling of two-dimensional quantum spin glasses.
Phys. Rev. B, 94, 024201 (2016).
53. O. Motrunich, S.-C. Mau, D. A. Huse, et al.
Infinite-randomness quantum Ising critical fixed points.
Phys. Rev. B, 61, 1160 (2000).
54. D. Karevski, Y.-C. Lin, H. Rieger, et al.
Random quantum magnets with broad disorder distribution.
Eur. Phys. J. B, 20, 267 (2001).
55. Y.-C. Lin, F. Iglói, and H. Rieger.
Entanglement Entropy at Infinite-Randomness Fixed Points in Higher Dimensions.
Phys. Rev. Lett., 99, 147202 (2007).
56. F. Iglói and C. Monthus.
Strong disorder RG approach of random systems.

- Phys. Rep.*, 412, 277 (2005).
57. F. Iglói and C. Monthus.
Strong disorder RG approach – a short review of recent developments.
Eur. Phys. J. B, 91, 290 (2018).
 58. G. Parisi.
The order parameter for spin glasses: a function on the interval 0-1.
J. Phys. A: Math. Gen., 13, 1101 (1980).
 59. K. Binder and A. P. Young.
Spin glasses: Experimental facts, theoretical concepts, and open questions.
Rev. Mod. Phys., 58, 801 (1986).
 60. A. P. Young.
Stability of the quantum Sherrington-Kirkpatrick spin glass model.
Phys. Rev. E, 96, 032112 (2017).
 61. S. Mukherjee, A. Rajak, and B. K. Chakrabarti.
Possible ergodic-nonergodic regions in the quantum Sherrington-Kirkpatrick spin glass model and quantum annealing.
Phys. Rev. E, 97, 022146 (2018).
 62. S. Mukherjee, A. Rajak, and B. K. Chakrabarti.
Classical-to-quantum crossover in the critical behavior of the transverse-field Sherrington-Kirkpatrick spin glass model.
Phys. Rev. E, 92, 042107 (2015).
 63. A. Rajak and B. Chakrabarti.
Quantum annealing search of Ising spin glass ground state (s) with tunable transverse and longitudinal fields.
Indian J. Phys., 88, 951 (2014).
 64. H. Leschke, C. Manai, R. Ruder, et al.
Existence of Replica-Symmetry Breaking in Quantum Glasses.
Phys. Rev. Lett., 127, 207204 (2021).
 65. P. M. Schindler, T. Guaita, T. Shi, et al.
A Variational Ansatz for the Ground State of the Quantum Sherrington-Kirkpatrick Model.
arXiv preprint arXiv:2204.02923 (2022).
 66. A. P. Young, S. Knysh, and V. N. Smelyanskiy.
First-Order Phase Transition in the Quantum Adiabatic Algorithm.
Phys. Rev. Lett., 104, 020502 (2010).
 67. T. Jörg, F. Krzakala, G. Semerjian, et al.
First-order transitions and the performance of quantum algorithms in random optimization problems.
Phys. Rev. Lett., 104, 207206 (2010).
 68. E. Barouch, B. M. McCoy, and M. Dresden.
Statistical mechanics of the XY model. I.
Phys. Rev. A, 2, 1075 (1970).
 69. S. R. White and A. E. Feiguin.
Real-Time Evolution Using the Density Matrix Renormalization Group.
Phys. Rev. Lett., 93, 076401 (2004).
 70. G. Vidal.
Efficient simulation of one-dimensional quantum many-body systems.
Phys. Rev. Lett., 93, 040502 (2004).
 71. R. Orús and G. Vidal.
Infinite time-evolving block decimation algorithm beyond unitary evolution.
Phys. Rev. B, 78, 155117 (2008).
 72. F. Pollmann, S. Mukerjee, A. G. Green, et al.
Dynamics after a sweep through a quantum critical point.
Phys. Rev. E, 81, 020101 (2010).
 73. A. D. King, S. Suzuki, J. Raymond, et al.
Coherent quantum annealing in a programmable 2000-qubit Ising chain.
arXiv preprint arXiv:2202.05847 (2022).
 74. H. F. Trotter.
On the product of semi-groups of operators.
Proc. Am. Math. Soc., 10, 545 (1959).

75. M. Suzuki.
Quantum statistical Monte Carlo methods and applications to spin systems.
J. Stat. Phys., 43, 883 (1986).
76. R. H. Swendsen and J.-S. Wang.
Nonuniversal critical dynamics in Monte Carlo simulations.
Phys. Rev. Lett., 58, 86 (1987).
77. T. Nakamura and Y. Ito.
A quantum Monte Carlo algorithm realizing an intrinsic relaxation.
J. Phys. Soc. Jpn., 72, 2405 (2003).
78. T. Kadowaki.
Study of Optimization Problems by Quantum Annealing (2002).
79. G. E. Santoro, R. Martonák, E. Tosatti, et al.
Theory of quantum annealing of an Ising spin glass.
Science, 295, 2427 (2002).
80. R. Martoňák, G. E. Santoro, and E. Tosatti.
Quantum annealing by the path-integral Monte Carlo method: The two-dimensional random Ising model.
Phys. Rev. B, 66, 094203 (2002).
81. R. Martoňák, G. E. Santoro, and E. Tosatti.
Quantum annealing of the traveling-salesman problem.
Phys. Rev. E, 70, 057701 (2004).
82. D. A. Battaglia, G. E. Santoro, and E. Tosatti.
Optimization by quantum annealing: Lessons from hard satisfiability problems.
Phys. Rev. E, 71, 066707 (2005).
83. S. Suzuki.
Kibble-Zurek mechanism in simulated annealing and quantum annealing.
In *J. Phys.: Conf. Ser.*, volume 302, page 012046. IOP Publishing (2011).
84. W. Wu, B. Ellman, T. F. Rosenbaum, et al.
From classical to quantum glass.
Phys. Rev. Lett., 67, 2076 (1991).
85. J. Brooke, D. Bitko, Rosenbaum, et al.
Quantum annealing of a disordered magnet.
Science, 284, 779 (1999).
86. S. Säubert, C. L. Sarkis, F. Ye, et al.
Microscopies of Quantum Annealing in the Disordered Dipolar Ising Ferromagnet $\text{LiHo}_x\text{Y}_{1-x}\text{F}_4$.
arXiv preprint arXiv:2105.03408 (2021).
87. A. Keesling, A. Omran, H. Levine, et al.
Quantum Kibble-Zurek mechanism and critical dynamics on a programmable Rydberg simulator.
Nature, 568, 207 (2019).
88. M. W. Johnson, M. H. Amin, S. Gildert, et al.
Quantum annealing with manufactured spins.
Nature, 473, 194 (2011).
89. V. S. Denchev, S. Boixo, S. V. Isakov, et al.
What is the Computational Value of Finite-Range Tunneling?
Phys. Rev. X, 6, 031015 (2016).
90. S. Boixo, T. F. Rønnow, S. V. Isakov, et al.
Evidence for quantum annealing with more than one hundred qubits.
Nat. Phys., 10, 218 (2014).
91. S. W. Shin, G. Smith, J. A. Smolin, et al.
How "quantum" is the D-Wave machine?
arXiv preprint arXiv:1401.7087 (2014).
92. S. Suzuki and A. Das.
Quantum annealing: The fastest route to quantum computation? (2015).
93. Y. Bando, Y. Susa, H. Oshiyama, et al.
Probing the universality of topological defect formation in a quantum annealer: Kibble-Zurek mechanism and beyond.
Phys. Rev. Research, 2, 033369 (2020).

94. D. Venturelli, S. Mandrà, S. Knysh, et al.
Quantum optimization of fully connected spin glasses.
Physical Review X, 5, 031040 (2015).
95. A. O. Caldeira and A. J. Leggett.
Quantum tunnelling in a dissipative system.
Ann. Phys. (N Y), 149, 374 (1983).
96. A. J. Leggett, S. Chakravarty, A. T. Dorsey, et al.
Dynamics of the dissipative two-state system.
Rev. Mod. Phys., 59, 1 (1987).
97. M. H. Amin.
Searching for quantum speedup in quasistatic quantum annealers.
Phys. Rev. A, 92, 052323 (2015).
98. D. Patanè, A. Silva, L. Amico, et al.
Adiabatic Dynamics in Open Quantum Critical Many-Body Systems.
Phys. Rev. Lett., 101, 175701 (2008).
99. D. Patanè, L. Amico, A. Silva, et al.
Adiabatic dynamics of a quantum critical system coupled to an environment: Scaling and kinetic equation approaches.
Phys. Rev. B, 80, 024302 (2009).
100. P. Nalbach, S. Vishveshwara, and A. A. Clerk.
Quantum Kibble-Zurek physics in the presence of spatially correlated dissipation.
Phys. Rev. B, 92, 014306 (2015).
101. A. Dutta, A. Rahmani, and A. del Campo.
Anti-Kibble-Zurek Behavior in Crossing the Quantum Critical Point of a Thermally Isolated System Driven by a Noisy Control Field.
Phys. Rev. Lett., 117, 080402 (2016).
102. P. Weinberg, M. Tylutki, J. M. Rönkkö, et al.
Scaling and Diabatic Effects in Quantum Annealing with a D-Wave Device.
Phys. Rev. Lett., 124, 090502 (2020).
103. M. Hasenbusch, K. Pinn, and S. Vinti.
Critical exponents of the three-dimensional Ising universality class from finite-size scaling with standard and improved actions.
Phys. Rev. B, 59, 11471 (1999).
104. M. Karl and T. Gasenzer.
Strongly anomalous non-thermal fixed point in a quenched two-dimensional Bose gas.
New J. Phys., 19, 093014 (2017).
105. M. Keck, S. Montangero, G. E. Santoro, et al.
Dissipation in adiabatic quantum computers: lessons from an exactly solvable model.
New J. Phys., 19, 113029 (2017).
106. S. Bandyopadhyay, S. Bhattacharjee, and A. Dutta.
Dynamical generation of Majorana edge correlations in a ramped Kitaev chain coupled to nonthermal dissipative channels.
Phys. Rev. B, 101, 104307 (2020).
107. D. Rossini and E. Vicari.
Dynamic Kibble-Zurek scaling framework for open dissipative many-body systems crossing quantum transitions.
Phys. Rev. Research, 2, 023211 (2020).
108. R. Puebla, A. Smirne, S. F. Huelga, et al.
Universal Anti-Kibble-Zurek Scaling in Fully Connected Systems.
Phys. Rev. Lett., 124, 230602 (2020).
109. L. Arceci, S. Barbarino, D. Rossini, et al.
Optimal working point in dissipative quantum annealing.
Phys. Rev. B, 98, 064307 (2018).
110. G. B. Mbeng, L. Arceci, and G. E. Santoro.
Optimal working point in digitized quantum annealing.
Phys. Rev. B, 100, 224201 (2019).
111. S. Suzuki, H. Oshiyama, and N. Shibata.
Quantum Annealing of Pure and Random Ising Chains Coupled to a Bosonic Environment.

- J. Phys. Soc. Jpn.*, 88, 061003 (2019).
112. H. Oshiyama, N. Shibata, and S. Suzuki.
Kibble–Zurek Mechanism in a Dissipative Transverse Ising Chain.
J. Phys. Soc. Jpn., 89, 104002 (2020).
 113. H. Oshiyama, S. Suzuki, and N. Shibata.
Classical simulation and theory of quantum annealing in a thermal environment.
Phys. Rev. Lett., 128, 170502 (2022).
 114. T. Jörg, F. Krzakala, J. Kurchan, et al.
Energy gaps in quantum first-order mean-field–like transitions: The problems that quantum annealing cannot solve.
EPL (Europhysics Lett.), 89, 40004 (2010).
 115. Y. Seki and H. Nishimori.
Quantum annealing with antiferromagnetic fluctuations.
Phys. Rev. E, 85, 051112 (2012).
 116. Y. Susa, Y. Yamashiro, M. Yamamoto, et al.
Exponential speedup of quantum annealing by inhomogeneous driving of the transverse field.
J. Phys. Soc. Jpn., 87, 023002 (2018).
 117. Y. Susa, Y. Yamashiro, M. Yamamoto, et al.
Quantum annealing of the p-spin model under inhomogeneous transverse field driving.
Phys. Rev. A, 98, 042326 (2018).
 118. H. Nishimori and G. Ortiz.
Elements of phase transitions and critical phenomena.
Oup Oxford (2010).
 119. B. Seoane and H. Nishimori.
Many-body transverse interactions in the quantum annealing of the p-spin ferromagnet.
J. Phys. A: Math. Theor., 45, 435301 (2012).
 120. M. Filippone, S. Dusuel, and J. Vidal.
Quantum phase transitions in fully connected spin models: An entanglement perspective.
Phys. Rev. A, 83, 022327 (2011).
 121. S. Matsuura, H. Nishimori, T. Albash, et al.
Mean field analysis of quantum annealing correction.
Physical review letters, 116, 220501 (2016).
 122. S. Matsuura, H. Nishimori, W. Vinci, et al.
Nested quantum annealing correction at finite temperature: p-spin models.
Physical Review A, 99, 062307 (2019).
 123. S. Knysh, E. Plamadeala, and D. Venturelli.
Quantum annealing speedup of embedded problems via suppression of Griffiths singularities.
Phys. Rev. B, 102, 220407 (2020).
 124. R. B. Griffiths.
Nonanalytic behavior above the critical point in a random Ising ferromagnet.
Phys. Rev. Lett., 23, 17 (1969).
 125. B. M. McCoy.
Incompleteness of the critical exponent description for ferromagnetic systems containing random impurities.
Phys. Rev. Lett., 23, 383 (1969).
 126. K. Jałowiecki, A. Więckowski, P. Gawron, et al.
Parallel in time dynamics with quantum annealers.
Sci. Rep., 10, 1 (2020).
 127. N. A. Aadit, A. Grimaldi, M. Carpentieri, et al.
Massively parallel probabilistic computing with sparse Ising machines.
Nat. Electron., pages 1–9 (2022).
 128. E. Pelofske, G. Hahn, and H. N. Djidjev.
Parallel quantum annealing.
Sci. Rep., 12, 1 (2022).
 129. D. Guéry-Odelin, A. Ruschhaupt, A. Kiely, et al.
Shortcuts to adiabaticity: Concepts, methods, and applications.
Rev. Mod. Phys., 91, 045001 (2019).

130. D. Sels and A. Polokovnikov.
Minimizing irreversible losses in quantum systems by local counterdiabatic driving.
Proc. Natl. Acad. Sci., 114, E3909 (2017).
131. A. D. King, J. Raymond, T. Lanting, et al.
Quantum critical dynamics in a 5000-qubit programmable spin glass (2022).
132. N. Mohseni, P. L. McMahon, and T. Byrnes.
Ising machines as hardware solvers of combinatorial optimization problems.
Nature Reviews Physics, 4, 363 (2022).
133. R. Harris, Y. Sato, A. J. Berkley, et al.
Phase transitions in a programmable quantum spin glass simulator.
Science, 361, 162 (2018).
134. P. Kairys, A. D. King, I. Ozfidan, et al.
Simulating the shastry-sutherland ising model using quantum annealing.
Phys. Rev. X Quantum, 1, 020320 (2020).
135. A. D. King, C. D. Batista, J. Raymond, et al.
Quantum annealing simulation of out-of-equilibrium magnetization in a spin-chain compound.
Phys. Rev. X Quantum, 2, 030317 (2021).
136. A. Mott, J. Job, J.-R. Vlimant, et al.
Solving a Higgs optimization problem with quantum annealing for machine learning.
Nature, 550, 375 (2017).
137. S. Das, A. J. Wildridge, S. B. Vaidya, et al.
Track clustering with a quantum annealer for primary vertex reconstruction at hadron colliders.
arXiv preprint arXiv:1903.08879 (2019).
138. S. Abel and M. Spannowsky.
Quantum-Field-Theoretic Simulation Platform for Observing the Fate of the False Vacuum.
Phys. Rev. X Quantum, 2, 010389 (2021).
139. A. Teplukhin, B. K. Kendrick, and D. Babikov.
Calculation of molecular vibrational spectra on a quantum annealer.
J. Chem. Theory Comput., 15, 4555 (2019).
140. A. Perdomo-Ortiz, N. Dickson, M. Drew-Brook, et al.
Finding low-energy conformations of lattice protein models by quantum annealing.
Sci. Rep., 2, 1 (2012).
141. R. Y. Li, R. Di Felice, R. Rohs, et al.
Quantum annealing versus classical machine learning applied to a simplified computational biology problem.
NPJ quantum information, 4, 1 (2018).
142. M. H. S. Amin, P. J. Love, and C. J. S. Truncik.
Thermally Assisted Adiabatic Quantum Computation.
Phys. Rev. Lett., 100, 060503 (2008).
143. N. G. Dickson, M. W. Johnson, M. H. Amin, et al.
Thermally assisted quantum annealing of a 16-qubit problem.
Nat. Commun., 4, 1903 (2013).
144. A. Mishra, T. Albash, and D. A. Lidar.
Finite temperature quantum annealing solving exponentially small gap problem with non-monotonic success probability.
Nat. Commun., 9, 2917 (2018).
145. V. Bapst and G. Semerjian.
On quantum mean-field models and their quantum annealing.
J. Stat. Mech.: Theory Exp., 2012, P06007 (2012).